Indo-Pacific Ocean response to atmospheric intraseasonal variability: 2. Boreal summer and the Intraseasonal Oscillation

Duane E. Waliser
Marine Sciences Research Center, State University of New York at Stony Brook, Stony Brook, New York, USA

Ragu Murtugudde
Earth System Science Interdisciplinary Center, University of Maryland, College Park, Maryland, USA

Lisanne E. Lucas
Marine Sciences Research Center, State University of New York at Stony Brook, Stony Brook, New York, USA

Received 11 June 2003; revised 29 November 2003; accepted 13 January 2004; published 19 March 2004.

[1] The basin-wide response of the Indo-Pacific Ocean to atmospheric forcing associated with the Intraseasonal Oscillation (ISO) is examined using an ocean general circulation model forced by canonical ISO conditions constructed from observations. The results show that the imposed ISO forcing induces ocean variability that both is local to the region of intense convective activity and has considerable variability outside this region. In the areas most strongly and directly affected by ISO forcing, mixed layer depth variations were found to be considerable and tended to contribute positively to the magnitude of the sea surface temperature (SST) variations. In addition, there are a number of places where variations in entrainment and three-dimensional ocean advection make nontrivial contributions to the mixed layer heat budget. Large values of entrainment variability in the Bay of Bengal signify one noteworthy difference between this and the austral summer case, which showed no large-scale ocean regions exhibiting significant entrainment variability. The ISO-related intraseasonal variability that occurred in regions remote from the ISO forcing include SST variability in the equatorial eastern Pacific that was generally analogous to the eastern Pacific variability associated with the austral summer case. ISO wind stress forcing induces remotely forced sea level variations, via Kelvin waves, on the equator and the eastern sides of the Indian and Pacific basins. In the case of the Indian Ocean these variations are on the order of 5–10 cm and travel in a matter of weeks from the central basin well into the Bay of Bengal as well as southward along Java and into the Indonesian seas. In conjunction with these sea level variations are variations in basin-wide transports. Specifically, variations in the Indonesian Throughflow (ITF) brought about by ISO forcing are of the same order of magnitude as the seasonal cycle of ITF transport ($\sim$1 PW; 10 Sv). In contrast, the variations associated with the climatological cross-equatorial flow in the Indian Ocean basin are considerably larger ($\sim\pm$2 PW; 20 Sv) than those associated with ISO forcing ($\sim\pm$0.2 PW; 2 Sv). The results also showed that the imposed ISO forcing and associated ocean response exhibit a low-frequency rectification, namely a mean SST warming ($\sim$0.1°C) and MLD shoaling ($\sim$7 m) over much of the northern Indian and northwestern tropical Pacific Oceans. The implications and caveats associated with the above results, the caveats associated with the model and forcing framework, and the areas necessitating further study are discussed. *INDEX TERMS:* 3339 Meteorology and Atmospheric Dynamics: Ocean/atmosphere interactions (0312, 4504); 3337 Meteorology and Atmospheric Dynamics: Numerical modeling and data assimilation; 3374 Meteorology and Atmospheric Dynamics: Tropical meteorology; 1620 Global Change: Climate dynamics (3309); 4215 Oceanography: General: Climate and interannual variability (3309); *KEYWORDS:* climate, ocean modeling, Madden-Julian Oscillation

Citation: Waliser, D. E., R. Murtugudde, and L. E. Lucas (2004), Indo-Pacific Ocean response to atmospheric intraseasonal variability: 2. Boreal summer and the Intraseasonal Oscillation, *J. Geophys. Res.*, *109*, C03030, doi:10.1029/2003JC002002.

0148-0227/04/2003JC002002$09.00

1. Introduction

[2] *Waliser et al.* [2003] (hereinafter referred to as WML) examined the basin-scale ocean response to atmospheric intraseasonal variability (ISV) during austral summer, namely, the Madden-Julian Oscillation (MJO). The background and motivation for undertaking these two studies was addressed in great detail by WML and thus most of that material (including the supporting references) will not be repeated here. In short, WML emphasized the importance of tropical atmospheric ISV, both in terms of its local impact on weather and short-term climate in the tropical eastern hemisphere, as well as its remote impacts on the eastern Pacific Ocean, and on weather and short-term climate in the midlatitudes, particularly around the Americas. In addition, given the shortcomings in the representation of ISV in atmospheric general circulation models, along with results from a number of studies that suggest that near-surface ocean coupling may play some role in achieving a proper physical representation of this variability, a better understanding of the ocean response to atmospheric ISV is needed. This includes not only understanding general questions concerning the magnitude and spatial variability of the ocean response and how that may play a role in the coupled component of atmospheric ISV, but also determining which components of the atmospheric forcing are most important, how much and where does ocean advection play a role in the ocean response, is there important remotely forced ocean variability that occurs in conjunction with atmospheric ISV, to what degree are basin-scale transports modulated by ISV, and does the ocean response involve any rectification of the intraseasonal timescale onto longer timescales? The present line of research has been undertaken to try to address these sorts of questions. Since the character of atmospheric ISV, and in particular the regions of the ocean that it directly impacts, is strongly dependent on season [e.g., *Wang and Rui*, 1990; *Jones et al.*, 2003], this study was broken into two components. WML examined the ocean response under austral summer conditions when ISV typically takes the form of the MJO, which involves convective anomalies that propagate eastward from the Indian Ocean, across the Maritime Continent and western Pacific, and into the South Pacific Convergence Zone (SPCZ). In this study, we examine the ocean response under boreal summer conditions when intraseasonal convective events, often referred to as Intraseasonal Oscillations (ISOs; in some cases these are simply referred to as boreal summer MJOs), tend to propagate northeastward from the Indian Ocean across Southeast Asia, into the northwestern Tropical Pacific Ocean. As with WML, this component of the study tends to focus mostly on the Indo-Pacific warm pool regions where the ISO-related forcing and associated ocean response is greatest. Moreover, it is worth reiterating that this study employs an ocean general circulation model (OGCM) as the main tool for investigation because of the paucity of relevant ocean observations, particularly when considering ocean dynamical processes as well as a basin-wide perspective. The model formulation is described in section 2. Section 3 describes the experimental setup, the procedures used to develop the ISO forcing conditions, and some validation analysis of the model's representation of intraseasonal variations. Section 4 describes the results and section 5 presents a brief summary of the results along with a discussion of their implications, the questions they raise and suggestions for future work.

2. Model

[3] The modeling framework is identical to WML, with one exception described below, and thus will not be repeated here. Since the bulk of the intraseasonal activity associated with the Northern Hemisphere summer occurs near the southeast Asian continent, a region where riverine discharge is known to have an important impact on surface hydrography and mixed layer processes [e.g., *Han and McCreary*, 2001; *Howden and Murtugudde*, 2001] we have incorporated riverine impacts into the climatological forcing for this area. For this purpose, climatological riverine discharges were obtained from the UNESCO report [*Burton*, 1988] and are included as a estuarine boundary exchange at the proximate locations of the river mouths with an assumption that the discharge occurs between 1 to 2 degrees of latitude or longitude depending on the river [see *Han and McCreary*, 2001]. The salinity of the emerging river water is approximated on the basis of the climatological July surface salinities from *Levitus* [1994]. No enhanced vertical mixing is applied in the vicinity of the river mouths. This methodology is found to simulate the effects of rivers better than our previous method of incorporating the discharges as freshwater fluxes [*Howden and Murtugudde*, 2001; *Delcroix and Murtugudde*, 2002].

3. Data and Experimental Setup

3.1. Climatological Forcing and Setup

[4] The climatological forcing and associated model spin-up are identical to WML. WML give and discuss the annual mean model sea surface temperature (SST) and associated bias relative to observations. In this case, since the focus is on Northern Hemisphere summer, Figure 1 illustrates the modeled and the difference between the modeled and observed [*Levitus*, 1994] May–August mean SSTs. Similar to the austral summer case, there is a warm bias in the Indo-Pacific warm pool region and a cold bias in the eastern equatorial Pacific Ocean. This sort of bias structure and its potential underlying causes are discussed by WML. As with that study, there are three main points to emphasize regarding the model climatology, at least in terms of SST: 1) the bias over most of the Indo-Pacific region is on the order of 1° or less which suggests that the model is adequately depicting the basin-scale climatology, 2) the study framework relies primarily on the ocean model's anomalous response rather than on the climatological structure - albeit the two are not independent, and 3) sensitivity tests using an imposed flux bias correction to improve the near-surface climatology show that the main results of the study do not depend on the modest errors associated with the model's near-surface climatology.

3.2. ISO Forcing and Setup

[5] Ocean forcing conditions associated with the ISO were constructed using the same compositing approach as described by WML. Because of the importance of this

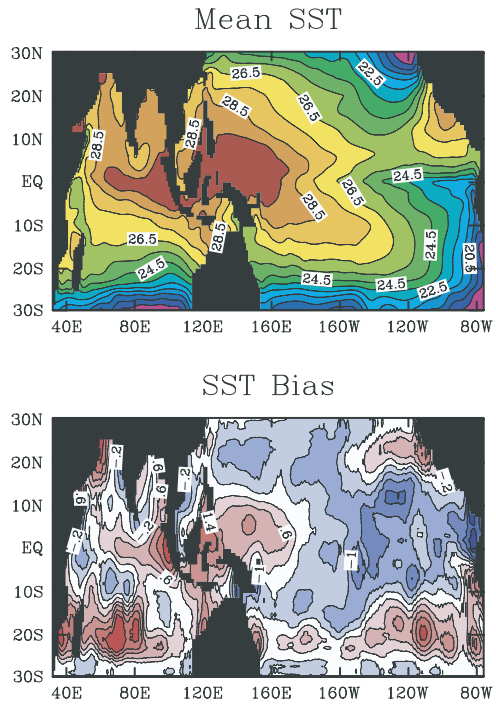

Figure 1. (top) Mean May–August sea surface temperature (SST) from the ocean model. (bottom) Difference between the model SST and observations [*Levitus*, 1994] for the same period.

procedure to the development and analysis of the study, and that it involves seasonal specific information, it will be described in detail below. ISO events were identified through extended EOF (EEOF) analysis of band-passed pentad (i.e., 5-day average) rainfall data [*Xie and Arkin*, 1997] that extends from 1979 to 1999. Band-pass filtering was performed using a 35–95-day Lanczos filter [*Duchon*, 1979]. In order to isolate the canonical form of the ISO, that which is most prevalent in boreal summer [*Wang and Rui*, 1990; *Ferranti et al.*, 1997; *Annamalai et al.*, 1999; *Sperber et al.*, 2000; *Jones et al.*, 2003], only Northern Hemisphere "summer" (hereafter, defined as May–October) data were retained in the analysis. From these band-passed summer data, EEOFs are computed for ±7 pentad time lags on the region between 30°E and 180°E. Figure 2 shows that the mode 1 pattern represents a northeastward propagating structure with about a 50-day period that is strongly reminiscent of a typical ISO evolution. Candidate events for constructing the ISO composite were selected when the value of the unit normalized amplitude time series of mode 1 exceeded 1.2. Figure 3 shows the amplitude time series of EEOF mode 1 (based on the EEOF mode projected back onto the entire time series of data) along with the candidate ISO events. Also shown on Figure 3 are the temporal extents of the additional forcing data sets that are used for constructing the composite ISO forcing. These additional data sets include the (1) daily SSM/I [*Atlas et al.*, 1996] winds for computing wind speed, direction, and stress; (2) daily ISCCP-derived surface shortwave values [*Bishop et al.*, 1997]; and (3) daily ISCCP-D-derived total cloud fraction [*Rossow and Schiffer*, 1991]. In each case, these additional forcing data sets were interpolated to pentads ($73\ yr^{-1}$) to match the temporal resolution of the rainfall data. Note that because of the nonoverlapping nature of the data sets, some composites contain fewer/different events (e.g., the shortwave (wind) includes events mostly from the 1980s (1990s)). In addition, daily values of wind speed and wind stress were first computed from the daily values of vector wind. These daily values were then used to define the associated climatologies and in turn the anomalies.

[6] For each forcing data set, the corresponding candidate ISO events were averaged to form a composite forcing structure with the same lags as the EEOF (i.e., Figure 2). For rainfall, shortwave, cloud fraction and wind, this involved 30, 10, 21, and 15 events respectively. As expected and as seen in Figure 2, the above forcing structures exhibit a cyclic structure with a repeating timescale of about 50 days. For example, the map in Figure 2 with lag −5 pentads is nearly the same as the map with lag +5 pentads. Thus a complete ISO cycle, which begins with a near-neutral rainfall anomaly in the western Indian Ocean, can be constructed using the 10 pentads between −4 pentads lag and +5 pentads lag. In addition, to overcome the decrease in the magnitude of the forcing associated with averaging over different candidate events, the composite forcing fields are multiplied by a scale factor (in this case 1.7). This compositing procedure produces forcing fields required by the OGCM and that are associated with a "typical" ISO (see Figures 4 and 5 and associated discussion below).

[7] In general, the above compositing procedure is applied to the band-passed data for each forcing field. This helps to prevent interannual variability from biasing the ISO forcing fields. However, it is important to note that even though these composites are roughly cyclic and are constructed from (intraseasonally) band-passed data, there is no constraint imposed, from either the methods used here or the observed system, that the time mean of the composites be zero at any given spatial location. For example, the convective phase of a typical ISO may involve slightly more westerly wind or a greater positive rainfall anomaly than occurs in the opposite sense for the subsidence phase. If this were the case, the balance would be made up during all the intervening periods between ISO events to give a zero anomaly for the total time series. The approach described above is an attempt to capture ISO event forcing conditions that are typical, realistic and ultimately based on observations. Examination of the composite ISO forcing shows that in fact they do exhibit small time mean values. These values are referred to as "residual" means and sensitivity tests to determine their impact are discussed in section 4. However, it is important to emphasize that this study is concerned with the ocean response to ISO conditions/events, not those associated with forcing from intervening periods. Composite forcing fields were also constructed using the unfiltered anomaly data. Not surprisingly, these anomaly based composites did exhibit nontrivial time mean values (i.e., "residual" mean) values that arose from the interannual (e.g., ENSO) variability within the data records. Thus these anomaly based composites were not used to represent ISO forcing but rather to provide a point of comparison for evaluating and describing the composites based on the filtered data.

[8] Since a number of ISO events often appear in sequence (e.g., Figure 3), the composite event can be concatenated together to form an idealized sequence of ISO

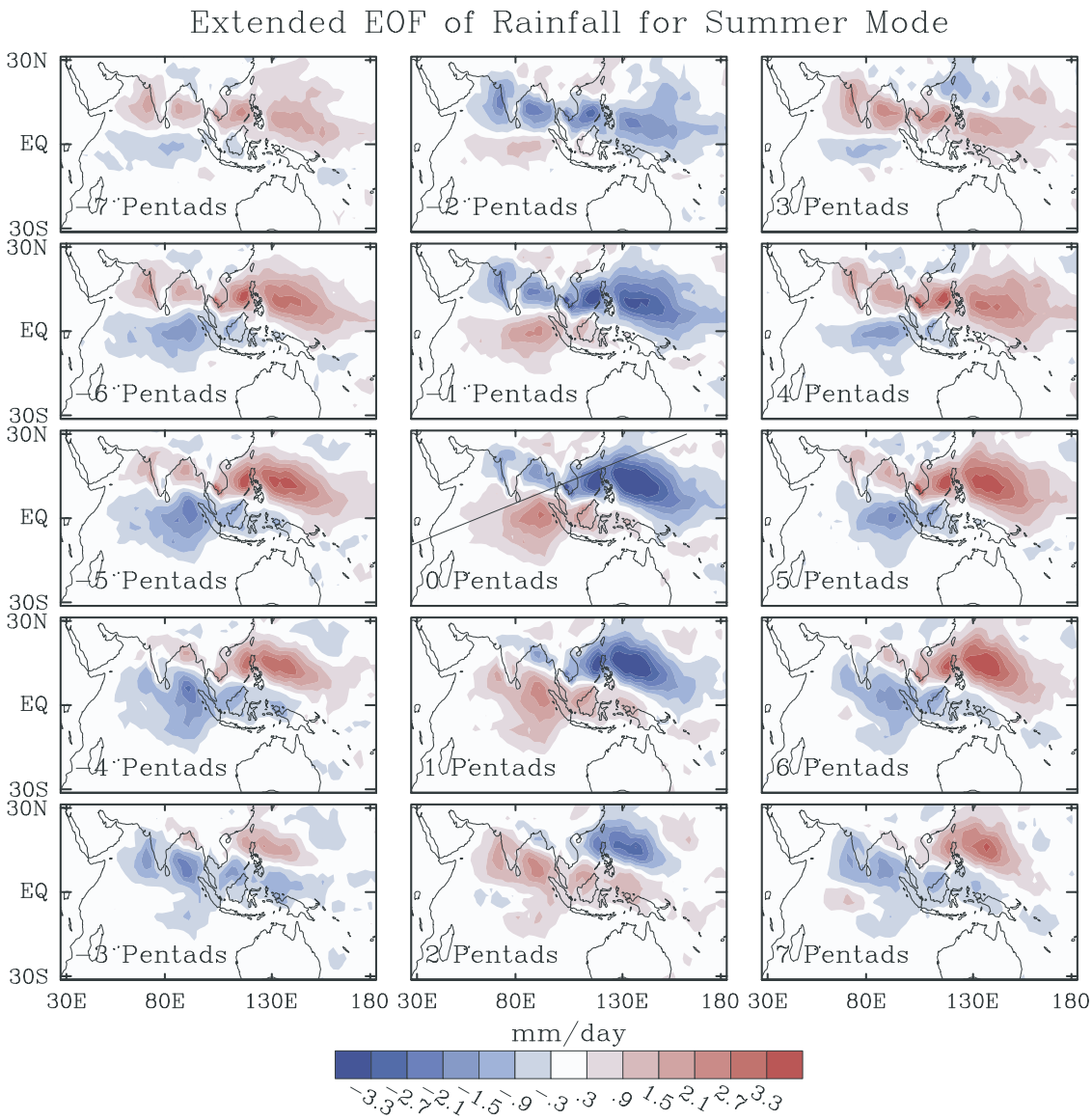

Figure 2. First-mode extended empirical orthogonal function (EEOF) of filtered (35–95 days) Boreal summer (May–October) rainfall for the tropical domain shown from the pentad values of *Xie and Arkin* [1997]. Time lags extend from −35 days (i.e., −7 pentads) in the upper left corner to +35 days (i.e., +7 pentads) in the lower right corner.

events. However, it should be kept in mind that because of the timescale of the ISO and the length of the period of the year when the canonical form of the ISO is most strongly exhibited (∼May–Septmber), only about 3–4 events can be expected to occur in any given summer season. Figure 4 illustrates a sequence of four composite ISO events in terms of space-time diagrams of rainfall, zonal wind, and surface shortwave. Note that the spatial dimension shown on the *x* axis of these plots is associated with the diagonal line shown in the middle panel of Figure 2. The temporal extent of the composite sequence is 230 days (= 46 pentads); this includes four 10-pentad ISO cycles plus 3 pentads at the beginning (end) of the sequence which contain 0, 1/3, and 2/3 (2/3, 1/3, and 0) times the first (last) perturbation value. Figure 2 (left) show composite events that were constructed from band-passed data while those on the right show composites constructed from anomaly (i.e., unfiltered) data. Note that the significant similarity between the band-passed and anomaly composites illustrates that the intraseasonal timescale of the phenomena is exhibited naturally in the data and not imposed by the band-pass operation. The analogous diagrams for wind stress and speed (not shown) look very similar to the zonal wind diagram with minima and maxima on the order ±0.5 dyne cm^{-2} and ±2 m s^{-1}. Similarly, the diagram for cloud fraction closely resembles the rainfall diagram but with minima and maxima of about ±0.20. To illustrate that the magnitude and character of the composite structure are reminiscent of observed events, Figure 5 shows pentad anomaly and band-passed rainfall data from the equatorial Indian and northwest tropical Pacific Oceans for three summer periods, along with the corresponding data from the composite ISO (i.e., Figure 4). A comparison of these plots demonstrates that the amplitude of the composite events (and thus the use of the above scale factor) is typical of

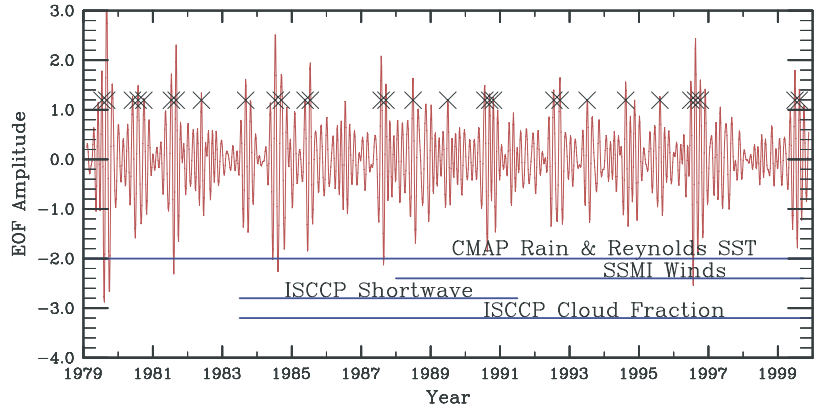

Figure 3. Amplitude time series for the first EEOF mode of filtered (35–95 days) Boreal summer rainfall (see Figure 2). The crosses represent ISO events selected for inclusion in the composite forcing. Horizontal lines and associated labels give the period encompassed by the given forcing and validation data sets. See section 3 for details.

observed events and that the constructed sequence of events is not too dissimilar from what is exhibited by the observations. In addition, the magnitude and nature of the composite ISO forcing conditions used here show a fair degree of similarity of those documented by BOBMEX [*Bhat*, 2001] over the Bay of Bengal (BoB).

[9] To succinctly illustrate the spatial variability associated with the ISO forcing, Figure 6 shows the standard

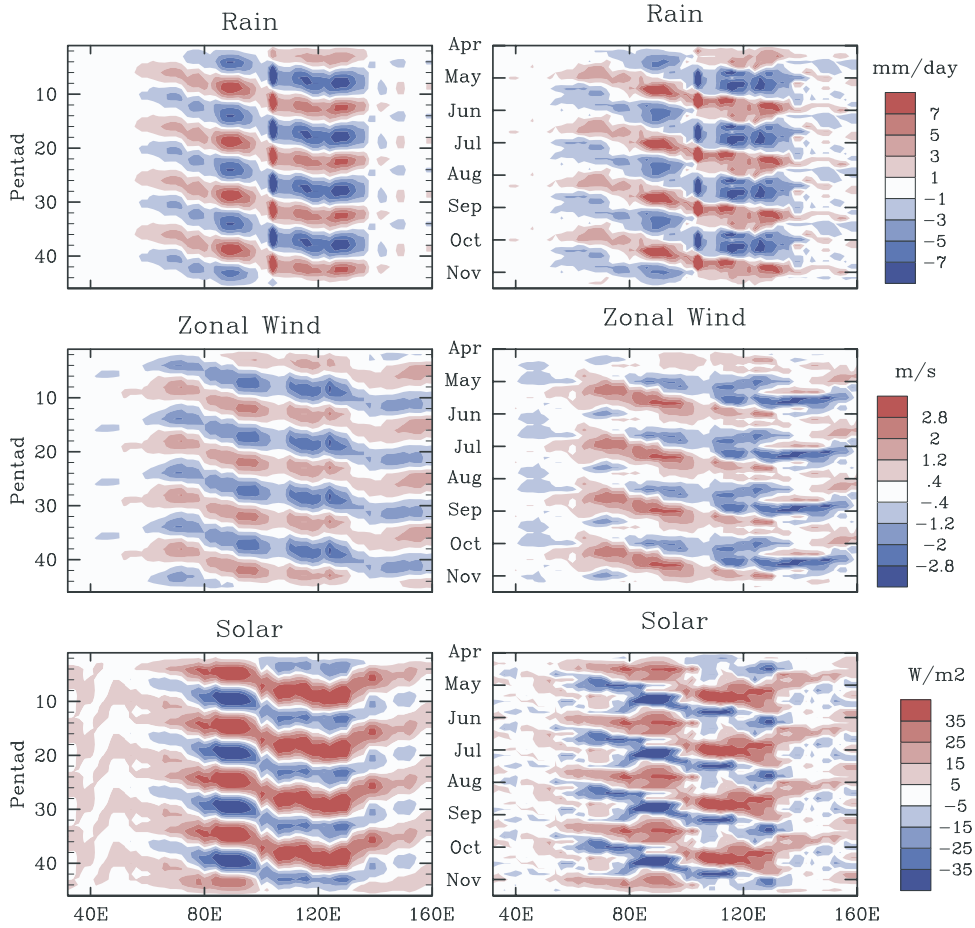

Figure 4. Time-space diagrams of ocean model forcing fields associated with a sequence of four canonical ISO events produced from (left) composites of band-passed (35–95 days) and (right) total anomaly (top) rainfall, (middle) zonal wind, and (bottom) surface shortwave radiation. Note that the *y* axis labels are given both in terms of pentads and calendar year when the anomalous forcing is applied. The latitude/longitude locations associated with the horizontal axis lie along the diagonal line shown in the middle panel of Figure 2.

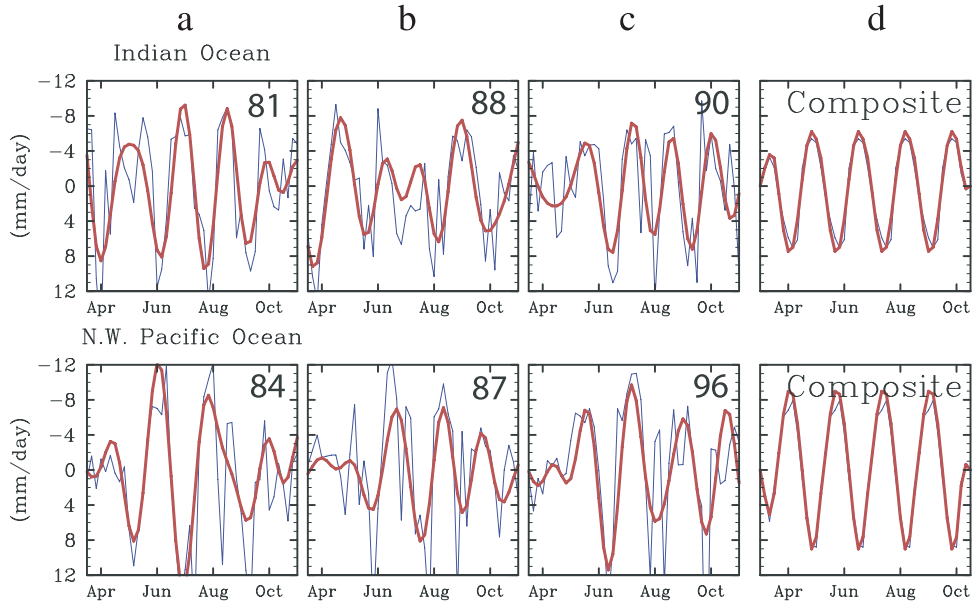

Figure 5. (a)–(c) Band-passed (35–95 days; thick) and total pentad (thin) rainfall anomalies for three Boreal summers over (top) the near-equatorial Indian Ocean (1°–11°N; 100°–110°E) and (bottom) the northwestern tropical Pacific (11°–21°N; 138°–148°E). (d) Sequence of four canonical ISO events produced from composites of band-passed (thick) and total anomaly (thin) rainfall data.

deviation of the composite ISO based on band-passed data. The analogous patterns associated with composites based on anomaly data (not shown) are nearly the same except that the magnitude is increased by about 10–15%. This, as well as the above comparisons between the band-passed and anomaly composites, indicates that the use of band-pass filtering to construct the ISO forcing had the desired effect of limiting the potential for interannual bias, and did not

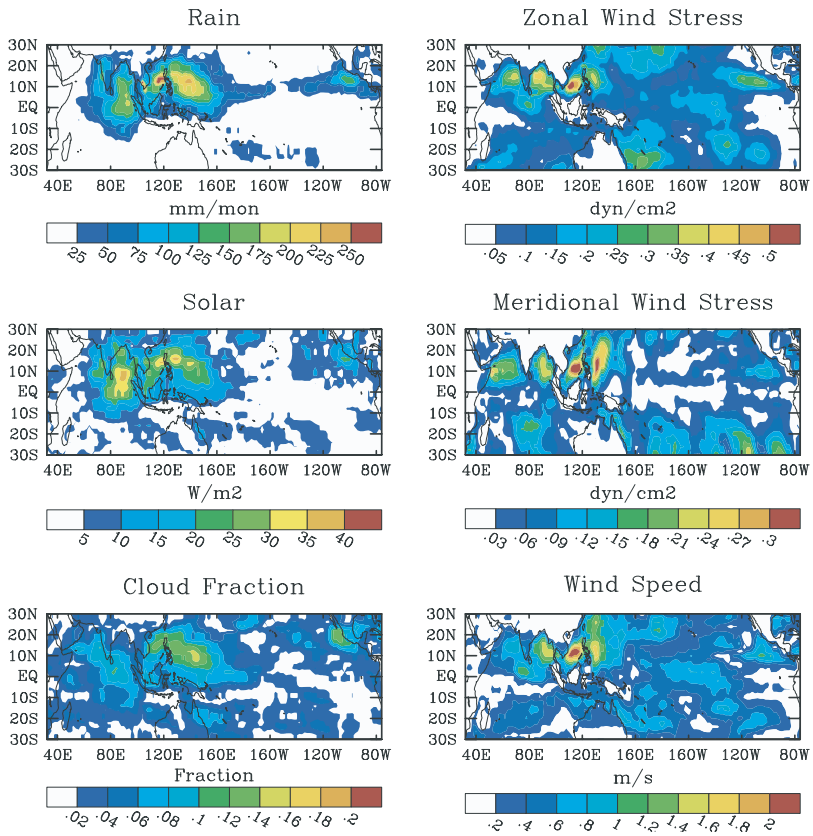

Figure 6. Standard deviation of the composite ISO forcing fields produced from band-passed (35–95 days) data. See section 3.2.

impose a timescale artificially or significantly change the spatial structure or magnitude of the variability. The maps in Figure 6 provide an indication of the regions where one would expect to find a local ocean response to the imposed ISO forcing. Note that because of the seasonal influences on the ISO, most of the forcing maxima are contained between about 5°S and 20°N with the zonal wind stress and wind speed more tightly confined than the forcing associated with clouds and precipitation. In addition, it is worth noting that there is relatively high wind stress variability in several regions of the subtropics as well. In contrast to the austral summer case where most of the wind stress variability was associated with the zonal component, and located near the equator, the boreal summer case exhibits co-located regions of somewhat larger amplitude zonal and meridional wind stress variability in and around the southeast Asian sector. This variability in both the zonal and meridional components is associated with the alternating cyclonic and anticyclonic ISO flow patterns [e.g., *Ferranti et al.*, 1997; *Annamalai et al.*, 1999; *Sperber et al.*, 2000]. In the discussion below, we will present similar figures associated with the ocean response to illustrate the mapping between the atmospheric forcing and the ocean response for the intraseasonal timescale.

[10] For the ISO simulations described in this study, the perturbation forcing fields associated with the composites were added to the climatological forcing fields and then used to force the ocean model. The perturbations were added such that the ISO forcing illustrated by Figure 4 begins on 1 April. From 1 April the simulations were integrated for one year. In such a case, the ISO is active between April and mid-November (i.e., 46 pentads), after which the forcing returns to its climatological values. The ocean response to intraseasonal forcing was then measured and described by the difference between the simulations with ISO forcing and the simulations using only climatological forcing. This presumes that there is no climatological ISO in the climatological forcing data [cf. *Wang and Xu*, 1997; *Kang et al.*, 1999], which is the case given that all the annual cycle forcing was computed from mean monthly data. Note that as with WML, a 4 m s^{-1} lower threshold is applied to the climatological wind speed values and the perturbation wind speed from the composite is added to the climatological value without applying an additional threshold (see section 3.1 of WML). Thus for the suppressed (wind speed) phase of ISO, the total wind speed can and does fall below the 4 m s^{-1} threshold that was applied to the climatological forcing. Given the 4 m s^{-1} threshold in the climatology and the size of the composite ISO wind fluctuations, the wind speed rarely falls below 2 m s^{-1} and never below 0.6 m s^{-1}. These very low wind speed cases (<2 m s^{-1}) occur in a few locations (approximately ten 2° × 2° model forcing grid points) in small regions around 20°N at both 110°E and 135°E over the course of 1–2 pentads during the low wind speed phase of the composite ISO cycle. With respect to rainfall, this low wind speed period occurs in association with lags +1 to +2 pentads of Figure 2. During this phase of the ISO cycle, the meridional wind over the above specified regions is anomalously northerly which when added to the generally southerly climatological flow in these regions (~3–6 m s^{-1}) results in a low wind phase of the ISO cycle. Finally, in addition to the ISO simulation that utilizes all of the forcing fields, hereafter referred to as the control, simulations were also performed that excluded one or more forcing fields. These additional simulations were performed to help diagnose the forcing mechanisms and associated processes responsible for various features in the simulated ocean response.

3.3. Validation Data and Methods

[11] To demonstrate that the model has a realistic representation of the near-surface ocean response to intraseasonal forcing it is useful to compare the model response to the observed response using anomalous forcing from a relatively active ISO period. For this purpose, weekly SST estimates from *Reynolds and Smith* [1994] were used to assess the fidelity of the large-scale intraseasonal ocean response. A full discussion of the methods and forcing data used for the "observed" forcing (1994–1999) simulation are described by WML. Figure 7 shows a comparison between the (band-passed) observed SST (left) along with the modeled values (right) in the form of time-longitude diagrams for the latitude band 8°–18°N during the boreal summers of 1996 and 1997. Note that this latitude band was chosen on the basis of the fact that the model exhibits the greatest amount of intraseasonal forced SST variability there (see Figure 8). The SST shows rather good model-data agreement during these periods, particularly west of the dateline, and east of 100°W where there is considerable local atmospheric forcing in terms of wind and cloud/solar-related variability (Figure 6). The only region of significant disagreement is in the eastern portion of the central Pacific Ocean. In this region the observations indicate the presence of westward propagating Rossby waves that the model does not capture. From Figure 6, it is evident that this variability is remotely forced as very little ISO-related forcing occurs locally in this part of the Pacific basin. In any case, this component of intraseasonal SST variability, which is related to the development of coastal jets off of the Tehuantepec peninsula in Central America and their generation of Rossby waves, does not seem to be well represented in the model, particularly when using winds that are not based on scatterometer data [*Hackert et al.*, 2001]. Another area of disagreement is along the eastern African coast. In this case however, it is very likely that the model's crude representation of the coastal/shelf geography is playing a significant role in the disagreement. Apart from these few caveats, the generally good model-data agreement described above, along with the additional agreement shown by WML, as well as previous uses of the same basic model to analyze the intraseasonal timescale [e.g., *Shinoda and Hendon*, 2001] demonstrate that the model exhibits a fair amount of fidelity at simulating the ocean response to intraseasonal forcing.

4. Results

4.1. Basin-Wide Ocean Response

[12] Figures 8 and 9 show the model's overall basin-wide response to the applied ISO forcing. In order to describe the part of the response attributed only to the ISO, it is necessary to construct an estimate of the model's internal variability (i.e., when only forced by annual cycle forcing). To construct these estimates, the variances about the mean annual climatology were computed from the same 3-year

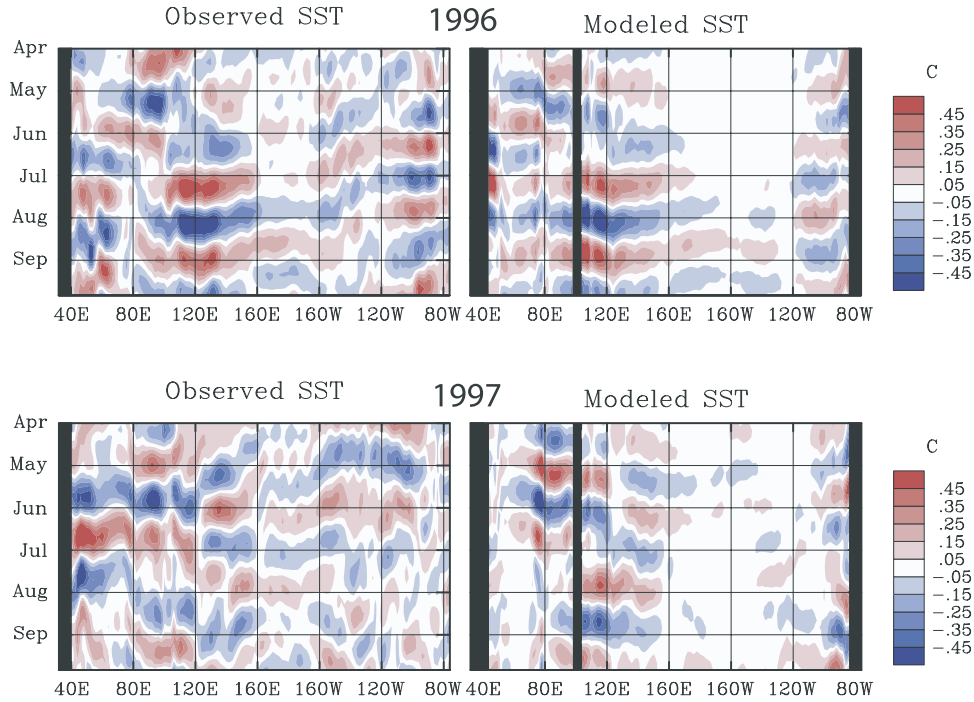

Figure 7. Time-longitude (8°–18°N) diagrams of intraseasonal SST variations during (top) 1996 and (bottom) 1997 from (left) observations [*Reynolds and Smith*, 1994] and (right) the model.

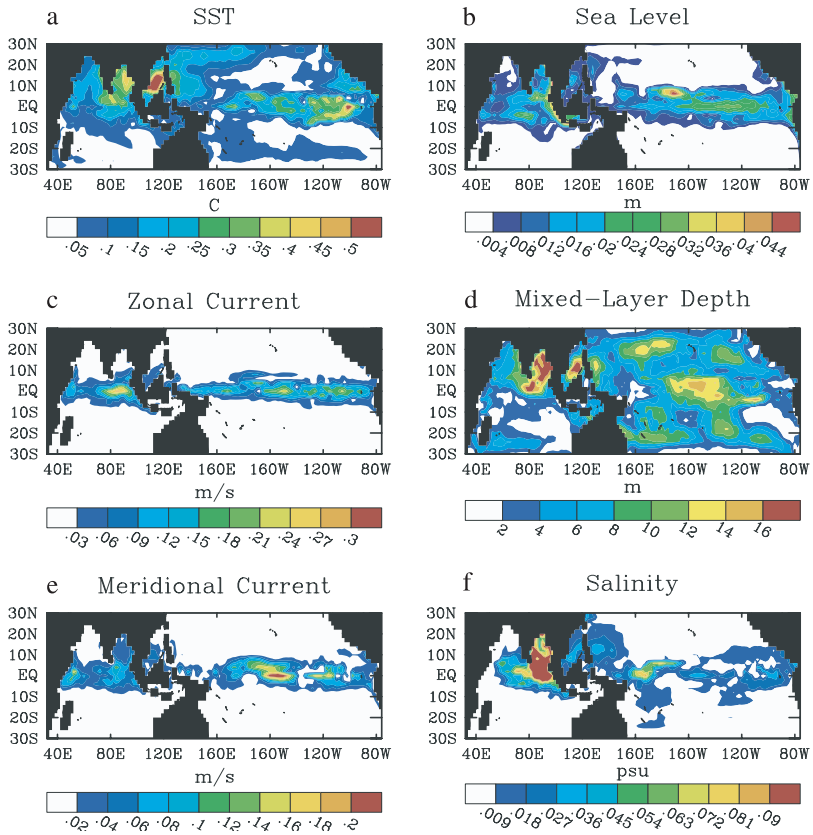

Figure 8. Estimate of the ocean model's response to ISO forcing, shown in terms of standard deviation. Values were calculated by first computing the differences between the ISO forcing case and the climatology. The variance of these differences (i.e., anomalous response) over the forcing period (April to late November) was computed and then the result associated with the internal variability (not shown; although Figure 9 of WML is nearly the same) was subtracted from this quantity.

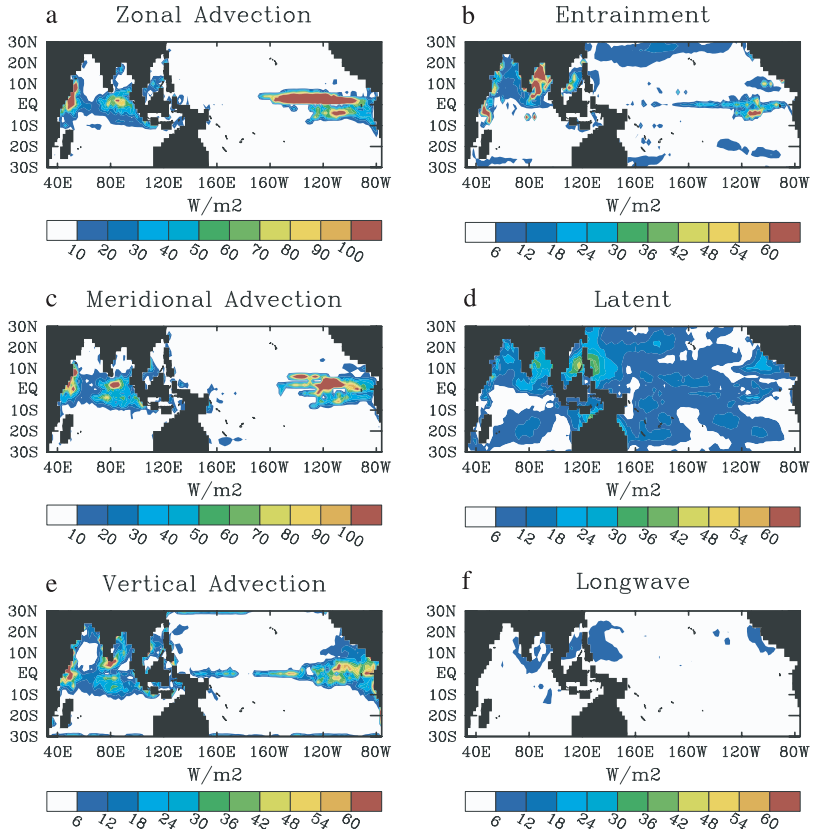

Figure 9. Same as Figure 8, except for quantities associated with the heat budget of the surface mixed layer.

period used to construct the climatology (see section 3.1 of WML). The average variance was then computed for the April through mid-November period (= 46 pentads). This variability is only associated with climatological forcing and thus can be ascribed to internal variability mechanisms in the model (e.g., Tropical Instability Waves (TIW)). To construct the maps shown in Figures 8 and 9, the anomalous response of the model was first determined by computing the differences between the ISO forcing case and the climatology. Then the variance of the anomalous response over the forcing period (April to mid-November) was computed. This variability contains both ISO forced variability and model internal variability. To estimate the part associated only with the ISO forcing, the background variability described above was subtracted from this quantity. For Figures 8 and 9, this resulting variance quantity is shown in terms of standard deviations. In addition, Figures 10 and 11 illustrate the ISO-forced SST and mixed layer depth (MLD) variability, respectively, for model simulations that had one of the anomalous ISO forcing components withheld.

[13] The estimate of the model's internal variability for the boreal summer season is similar enough to that associated with austral summer, which is given in Figure 9 of WML, that it will not be shown here. As with the austral summer case, the internal variability of the model during boreal summer is almost exclusively limited to the equatorial Pacific, most notably the central and eastern Pacific. In these regions SST, current, sea level, mixed layer depth and salinity variations are on the order: 0.5°C, 20 cm s^{-1}, 3 cm, 5 m, and 0.05 PSU. As with the austral summer case, this sort of variability is a result of the model's simulated TIWs. While the model estimates of the internal variability for the two seasons are quite similar, it is worth noting their two greatest differences. First, overall, the internal variability for most fields is weaker in the boreal summer case because of the seasonality of TIWs, although the differences are rather modest given the 7.5 month averaging windows used for computing this quantity in both the austral and boreal summer cases. Second, the regions of large internal variability extend westward to at least the dateline in the austral summer case but tend to be limited to the region east of about 160°W in the boreal summer case. Examination of maps associated with the internal variability of the heat budget terms for the surface mixed layer show that the internal SST variability that occurs in the equatorial Pacific is primarily a response to variations in meridional and zonal advection ($\sim\leq$300 and 150 Wm^{-2}, respectively), with modest contributions from vertical advection. ($\sim\leq$40 Wm^{-2}). Vertical entrainment and surface heat fluxes make minor contributions ($\sim\leq$20 Wm^{-2}), the latter of which results from the dependence of the turbulent and longwave fluxes on the model's SST itself.

[14] The maps in Figures 8 and 9 illustrate a rather wide range of influences associated with the added ISO forcing. The SST exhibits additional variability on the order of 0.3°–0.5°C in the northern Indian and northwestern tropical Pacific Ocean sectors, particularly near the South China Sea region [e.g., *Sengupta et al.*, 2001a; *Sengupta and Ravichandran*, 2001; *Vecchi and Harrison*, 2002; *Webster et al.*, 2002]. These areas are concomitant with

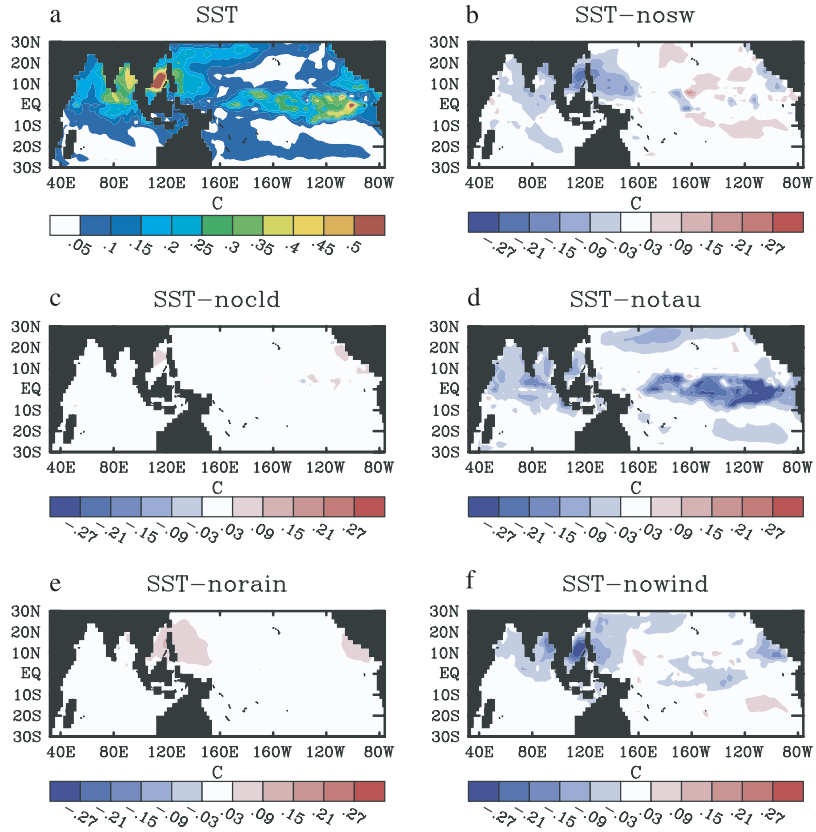

Figure 10. (a) Same as Figure 8a. (b)–(f) The difference between the plot analogous to Figure 10a but for a sensitivity simulation that did not include a given component of the ISO forcing and the plot for the control simulation (i.e., Figure 10a). The sensitivity simulations shown here include no anomalous ISO (Figure 10c) cloudiness, (Figure 10e) rainfall, (Figure 10b) shortwave, (Figure 10d) wind stress, and (Figure 10f) wind speed forcing.

the areas of largest local convection and wind forcing. More specifically, examination of Figure 6 and Figure 9 show that the SST variations in this region appear to be driven by variability in surface heat fluxes, mainly shortwave and latent heat flux ($\sim$25–50 Wm^{-2}), vertical mixed layer entrainment ($\sim$30–60 Wm^{-2}), and vertical advection ($\sim$10–15 Wm^{-2}), with very little contribution arising from horizontal advection. This represents one notable difference between the results here and those of WML, in that there were no large-scale regions in the WML study where entrainment played such a significant role determining SST variability. The nature of the entrainment variability in the BoB region will be discussed further in the next section. Examination of Figure 10 shows SST variability in the above regions is reduced by about 25%, 40% and 50% when ISO-related wind stress, shortwave and wind speed variations, respectively, are withheld. The latter case tests the impact of the latent and sensible perturbation forcing on response. The effects of withholding the wind stress in these northern Indian and northwestern Pacific Ocean regions are primarily associated with a reduction in entrainment that ranges anywhere between about a 30–100% reduction from what is exhibited in the control case shown in Figure 9. Similar reductions are found for this case for the horizontal and vertical advection - although these processes appear to play a less significant role than entrainment in determining SST variability in and around the BoB and South China Sea where the SST variations are largest.

[15] The results in Figure 10 show that withholding cloud variations, which affects only the net surface longwave in this experiment (as the net surface shortwave is specified as a separate/independent forcing), has almost no impact and for the most part withholding rainfall variations also has very little effect on SST with one exception. East of Indonesia, the SST variability is slightly greater when ISO-related variations in rainfall are withheld. This region exhibits very large rainfall perturbations (e.g., Figure 2) and these perturbations end up mitigating vertical mixing. For example, under disturbed (undisturbed) conditions, the case without rainfall perturbations has relatively less (more) rainfall than the case with ISO rainfall perturbations and this allows for slightly increased (decreased) vertical mixing which acts to enhance the cooling (warming) phase - thus leading to slightly larger SST variability. Support for this is evident in Figure 11 that shows slightly greater MLD variability in this region for the case without rainfall perturbations. Apart from the northern Indo-Pacific region discussed above, there is considerable forced variability exhibited in the far eastern Pacific Ocean. Figure 9 indicates that this variability is primarily driven by enhanced variability in zonal and meridional advection ($\sim\leq$150 Wm^{-2}) and to a lesser extent vertical advection and entrainment

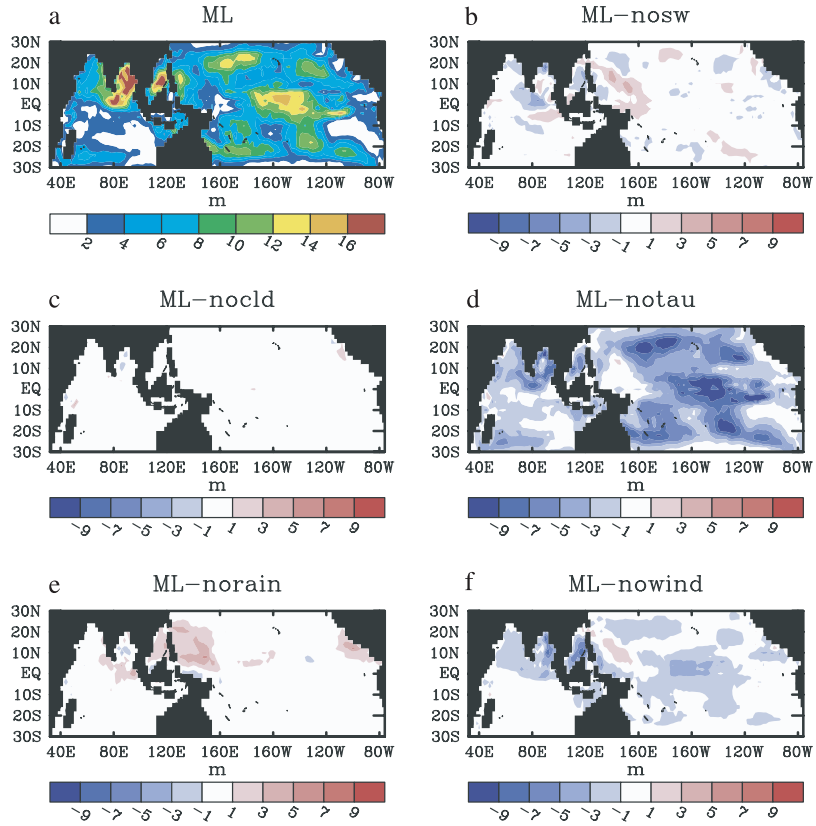

Figure 11. (a) Same as Figure 8d. (b)–(f) The difference between the plot analogous to Figure 11a but for a sensitivity simulation that did not include a given component of the ISO forcing and the plot for the control simulation (i.e., Figure 11a). The sensitivity simulations shown here include no anomalous ISO (Figure 11c) cloudiness, (Figure 11e) rainfall, (Figure 11b) shortwave, (Figure 11d) wind stress, and (Figure 11f) wind speed forcing.

($\sim \leq 50$ Wm^{-2}). Figure 10 demonstrates that this variability is almost exclusively a product of the wind stress forcing and in fact is qualitatively similar to the eastern Pacific SST variability discussed in more detail by WML. Because of this similarity, this aspect of the ocean response will not be treated further in this study and the reader is referred to WML. However, in regards to this component of the forced response, it is important to note that the basin-wide ocean response to canonical ISO forcing, as with the canonical MJO forcing discussed by WML, includes systematic variability remote from the main forcing region as well as the expected variability in the northern Indo-Pacific regions.

[16] MLD variability associated with the added ISO forcing extends over a fairly comprehensive area of the tropical Indian and Pacific basins. In the northern Indian Ocean, namely the BoB and to the south of it, as well as the South China Sea region, the variability brought about by the ISO forcing is about 15–20 m (in terms of standard deviation). Such variations are similar to that found in the recent JASMINE pilot field program [*Webster et al.*, 2002]. The manner in which these variations are related to the forcing will be described in more detail below. Apart from the above regions where the local ISO forcing is largest, there are other areas with somewhat comparable size MLD variability but with considerably less local ISO forcing (e.g., subtropics and eastern/central Pacific). These are regions that tend to exhibit little to no cloud and rainfall variability but do exhibit a modest amount of wind variability (Figure 6), and thus the MLD variability is associated with wind-induced mixing. Supporting evidence for this comes from simulations performed with the anomalous wind forcing excluded (Figure 11). Note that in the model, both wind stress (via mixing) and wind speed (via latent and sensible heat flux) have an impact on driving MLD variability in these remote regions, with the former being the primary driving mechanism. In fact in the case without ISO-related wind stress forcing, MLD variations are almost exclusively confined to the northern Indian and northwestern tropical Pacific Oceans. As with WML, examination of the subtropical MLD variability shows a fair degree of north-south symmetry, in that there are peak variations in both the southern and northern subtropics at around 20° latitude. However, the associated impact on SST is considerably smaller in the winter versus summer hemisphere because of the weaker stratification of the former. The processes associated with ISO/MJO-related SST variability in the wintertime subtropics are discussed in some detail by WML and thus will not be discussed again here. Rather in this study we provide a brief discussion, in the next section, on ISO-related SST variability in the summertime subtropics, namely that which occurs around 20°N and 160°E.

[17] The salinity variability associated with the ISO forcing (Figure 8f) occurs almost exclusively in the north-

ern Indian and northwestern tropical Pacific Oceans. While these salinity variations are relatively small compared to the model's mean salinity ranges, which extend from about 35.1 to 34.0 psu across the entire equatorial domain, they are relatively and locally large particularly in the region between the equator and the BoB. The sensitivity simulations with various anomalous forcing components withheld show that at least half of the ISO-related salinity variations in this region are a result of the anomalous wind stress variability. This implies that advection associated with anomalous currents and the mean salinity gradient is the main contributor. The latter arises because of the inclusion of freshwater riverine input into the BoB (see section 2) and the relatively large salinity gradients this establishes between the BoB and the equatorial region. It should be noted that identical simulations were run that did not contain the climatological riverine input and thus also did not exhibit these relatively and locally large salinity variations. Moreover, these simulations showed that these riverine inputs and associated salinity variability produced no qualitative changes to the behavior of the SST variability discussed above.

[18] Dynamic variability associated with the added ISO forcing is strongly constrained to the near-equatorial latitudes. This is expected given the spatial and temporal scales of the forcing and equatorial wave dynamics [e.g., *Matsuno*, 1966; *Cane*, 1979]. Apart from the direct ocean response in the Indian and western Pacific Ocean, which involves variability in surface zonal and meridional current on the order of 30 and 10 cm s^{-1}, respectively, there is ISO-related variability in the eastern Pacific associated with both enhanced TIW activity as well as the impacts from remotely forced equatorial Kelvin wave activity. These results are nearly identical to that found and discussed in more detail by WML. Here, we only highlight the principal differences between the austral and boreal summer cases. The main difference in the zonal current variability is that the variability in the western Pacific is weaker in the boreal summer case owing to the fact that the east-west surface wind variability is weaker for this case than for the austral summer case (compare Figure 6 with Figure 6 by WML). One of the main differences in the meridional current (as well as the sea level) variability are that the boreal summer case exhibits some weak variability around the BoB and South China Sea region while the austral summer case does not. This simply reflects the northern shift of the wind variability in the boreal summer case. Another difference in the meridional current is there is larger variability in the central/eastern Pacific Ocean near, and just to the north, of the equator. This reflects the model's enhanced TIW activity during the boreal summer period.

4.2. Detailed Ocean Response and Associated Processes

[19] Figures 12 and 13 show the space-time evolution of the ocean model response, in terms of SST, MLD, and surface current, to the applied ISO forcing. These maps are based on composites computed by averaging the model response over the four ISO events (i.e., Figure 4). The convention for the time lag shown in each panel of the figures is based on the canonical ISO rainfall pattern shown in Figure 2. Thus, on the basis of the discussion in section 3.2, each ISO event cycles through pentads −4 to +5 of the rainfall structure shown in Figure 2. The four panel sequences shown in Figures 12 and 13 correspond to lags −2, +0.5, +3, and +5.5 pentads. Note that a lag of +5.5 pentads implies, considering the cyclic nature of the forcing/process, the period between lag 5 and −4 pentads. These figures show that for the most part, the SST evolution through the equatorial Indian and northwestern tropical Pacific Oceans is as expected (see WML) [see also *Bhat*, 2001; *Kemball-Cook and Wang*, 2001; *Sengupta et al.*, 2001a; *Sengupta and Ravichandran*, 2001; *Vecchi and Harrison*, 2002]. While there is significantly less observational data available for MLD and surface currents in this region, the evolution of these quantities is also not inconsistent with expectations. The MLD tends to shoal (deepen) about 10−20 m during warm SST, low wind (cool SST, high wind) periods, and the equatorial zonal (meridional) surface currents oscillate between westward (divergent) and eastward (convergent) anomalies with a magnitude on the order of 30 (10) cm s^{-1}, the latter of which is consistent with observed values [e.g., *Knox*, 1976; *Luyten et al.*, 1980; *Knox*, 1981; *Schott et al.*, 1994; *Reppin et al.*, 1999]. A comparison with Figure 2 shows that negative (positive) anomalies in precipitation lead periods of positive (negative) anomalies in SST. In terms of the basin scale, it is worth noting that the ocean generally exhibits greater SST warming and MLD shoaling anomalies than SST cooling and MLD deepening anomalies; this is both in terms of spatial area affected and in the magnitude of the anomalies. This suggests a rectification effect of the ISO on the near surface ocean, an aspect that will be discussed in more detail below.

[20] To provide a more comprehensive picture of the evolution of the ocean response, specific locations will now be analyzed in more detail. These locations include the BoB (Figure 14), South China Sea (Figure 15), central equatorial Pacific Ocean (Figure 18), central Indian Ocean (just south of India), and the subtropical north central Pacific Ocean. Figures 14a, 15a, and 18a show the major components of the forcing; Figures 14b, 15b, and 18b show the response in terms of SST and MLD; Figures 14c, 15c, and 18c show the main contributing elements to the mixed layer heat budget (in Wm^{-3}, i.e., Wm^{-2} per meter of MLD); and finally, Figures 14d, 15d, and 18d show the components of the surface heat flux are (in Wm^{-2}). In the case of Figures 14c and 14d, 15c and 15d, and 18a and 18b, positive values indicate surface warming. In regards to the mixed layer heat budget, it should be noted that the asymmetry in the magnitude of the heating versus cooling arises because of the fact that the MLD is larger in the cooling phase. Note that consistent with the discussion of "residual" mean forcing in section 3.2, the time mean of the forcing data shown in the top panels of Figures 14a, 15a, and 18a are not necessarily exactly equal to zero.

[21] With respect to the BoB and South China Sea regions, the main elements of the forcing are derived from surface wind variations that impact the latent heat flux and ocean advection terms, and the rainfall and clouds that impact the surface shortwave (e.g., Figure 6) [see also *Bhat*, 2001; *Sengupta et al.*, 2001a; *Vecchi and Harrison*, 2002; *Webster et al.*, 2002]. In these two regions, during this time of year, the mean wind is southwesterly. Since the zonal and meridional wind anomalies are in phase they both positively contribute to the ISO-related variations in wind speed, and

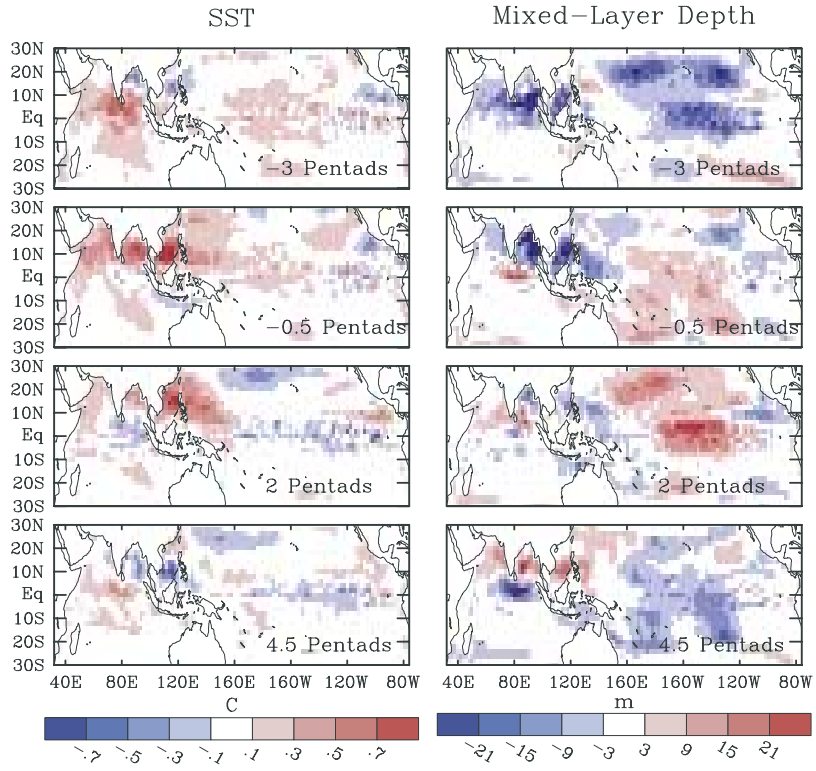

Figure 12. Composite ocean model response in terms of (left) SST and (right) mixed layer depth. The composites are computed by averaging the model response, at a given time lag relative to the ISO forcing, over the four ISO forcing events (i.e., Figure 4). The convention for the time lag, which is given in the lower right in each map, is based on the canonical ISO precipitation pattern shown in Figure 3. Note that a lag of −2 pentads occurs within the calendar year forcing at April P6, June P4, August P2, and September P6, where Pn is the pentad number for the given month ranging from 1 to 6. For lag +0.5 pentads, the dates are May P2.5, July P0.5, August P4.5, and October P2.5. For lag 3 pentads the dates are May P5, July P3, September P1, and October P5. For lag 5.5 pentads, the dates are June P1.5, July P5.5, September P3.5, November P1.5, and April 3.5.

thus determine the phase of the wind speed variations. This, in turn, determines the phase of the latent heat flux anomalies, which for these regions is the term in the surface heat flux budget that exhibits the largest variations. Since rainfall typically leads wind speed anomalies by about two pentads and also typically leads the peak in cloudiness (and thus shortwave) by one pentad for the composite ISO events, this makes the latent heat and surface shortwave (the second largest term in the surface heat flux budget) flux anomalies nearly in phase allowing them to constructively act together to heat and cool the ocean surface.

[22] The variations in net longwave radiation, which are considerably smaller, are out of phase with the shortwave and latent heat flux given that clouds increase the downward component of longwave radiation. The "Qnet Sum" term depicts the amount of shortwave energy lost out the bottom of the mixed layer. This term tends to be out of phase with the shortwave and latent heat flux because of the behavior of the MLD. Further, it tends to only exhibit negative values and these occur during periods of strong mixed layer shoaling; during other times the MLD is sufficiently deep (>40 m) to capture nearly all the shortwave energy. Note that the variations of MLD (as well as the SST) exhibited in the BoB (Figure 14b) are reasonably consistent with those documented during BOBMEX [*Bhat*, 2001]. This, along with the general model-data agreement in the phase and magnitude of the SST anomalies [e.g., *Sengupta and Ravichandran*, 2001; *Vecchi and Harrison*, 2002], provides some support that the model, along with the ISO forcing, used here appear to be properly accounting for the most important processes in this region. An additional feature worth noting is that during the period of ISO forcing, the MLD and SST exhibit a low-frequency modulation, namely the MLD (SST) is considerably shallower (warmer) over a given ISO cycle than the seasonal mean (i.e., that which would occur in the absence of ISO forcing) by about 10–20 m (0.5°C). This feature is consistent with the discussion above regarding the composites described in Figures 12 and 13.

[23] The results in Figures 14 and 15 show that for the BoB and South China Sea locations SST variations are primarily driven by surface heat flux, namely the latent heat and shortwave, and to a lesser extent net longwave and MLD variability interacting with shortwave penetration [e.g., *Sengupta and Ravichandran*, 2001]. Within these two regions, horizontal advection appears to play little role in determining the SST variability. For the case of the South China Sea, there is a modest contribution from zonal advection with warming occurring in conjunction with northeasterly wind anomalies. In this case, the main con-

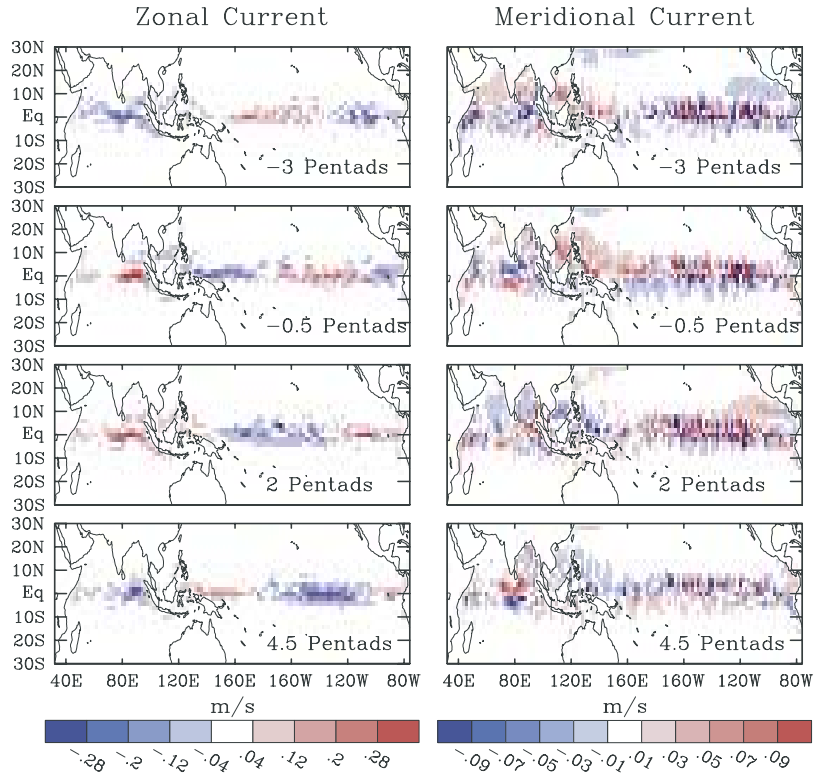

Figure 13. Same as Figure 12, except for surface (left) zonal and (right) meridional current.

tributor is associated with anomalous currents and the mean background SST, which from Figure 1 can be seen to have a positive zonal gradient between southeast Asia and Indonesia. While such a gradient does exist in the observed SST over most of the calendar year, it tends to be very small or nonexistent in the summer months and thus this contribution is likely to be overemphasized in the model. Another region that shows a relatively systematic contribution from dynamics to the SST variability is just south of India (3°–5°N; 81°–83°E). In this region, the surface heat budget exhibits a contribution from vertical advection (not shown) that is associated with coastal upwelling. During the easterly wind phase, the overall wind speed anomaly is negative and the surface heat flux anomaly is positive. The easterly wind suppresses the background upwelling and leads to increased warming, and vice versa for the westerly wind/cooling phase of the cycle. Most other features associated with this region are similar to the BoB except the forcing amplitude is weaker (see Figure 6) for wind and cloud related components and the MLD variations are much weaker (not shown).

[24] In regards to mixed layer entrainment, it is worth noting that even though there is relatively large variability in entrainment heat flux shown in Figure 9 for the BoB, there is a relatively small systematic contribution from this process to the surface heat budget over a given ISO cycle. This raises the question, why is the entrainment variability in the BoB so large in Figure 9. To understand this, it is instructive to first examine the evolution of the mixed layer processes in the BoB under climatological forcing and then consider the case with the additional ISO forcing. Figure 16 shows the evolution of the entrainment, MLD, surface layer buoyancy, and SST for the model climatology for the period from late July to mid-September (about one ISO cycle; compare with Figure 14). Under climatological forcing alone, large values of entrainment flux develop in the central BoB starting in early August and intensify and spread over the following month (Figure 16a). This enhanced entrainment flux is largely associated with changes in the mixed layer buoyancy characteristics (relative to the layer below; Figure 16c), which are in turn derived for the most part from the advection of relatively cool, and saline (not shown), water from the southwest (Figure 16d). It is worth mentioning that the model's spatial structure of SST in late July (i.e., pentad 5 of Figure 16a (top)) shows relatively good agreement with the observed mean July pattern [*Vecchi and Harrison*, 2002]; the agreement is even better when considering the model's mean July state (not shown). Note that even though the entrainment flux is relatively large, this occurs during a time when the MLD is actually shoaling (Figure 16b) because of a combination of an increase in the local net surface heat flux out of the ocean and the occurrence of shoaling of the local thermocline (not shown).

[25] Figure 17 shows how the ISO-forced case differs, in regards to the processes described above, from the case with only climatological forcing. The added ISO forcing produces substantial changes to the entrainment flux (Figure 17a). The most substantial of which occurs during mid-August to mid-September when the near surface water becomes extra buoyant relative to the layer below it. This occurs because of SST warming (middle-late August) as well as diminished salinity (late August to early September). This enhanced buoyancy, during the period that the mixed layer is anomalously warm

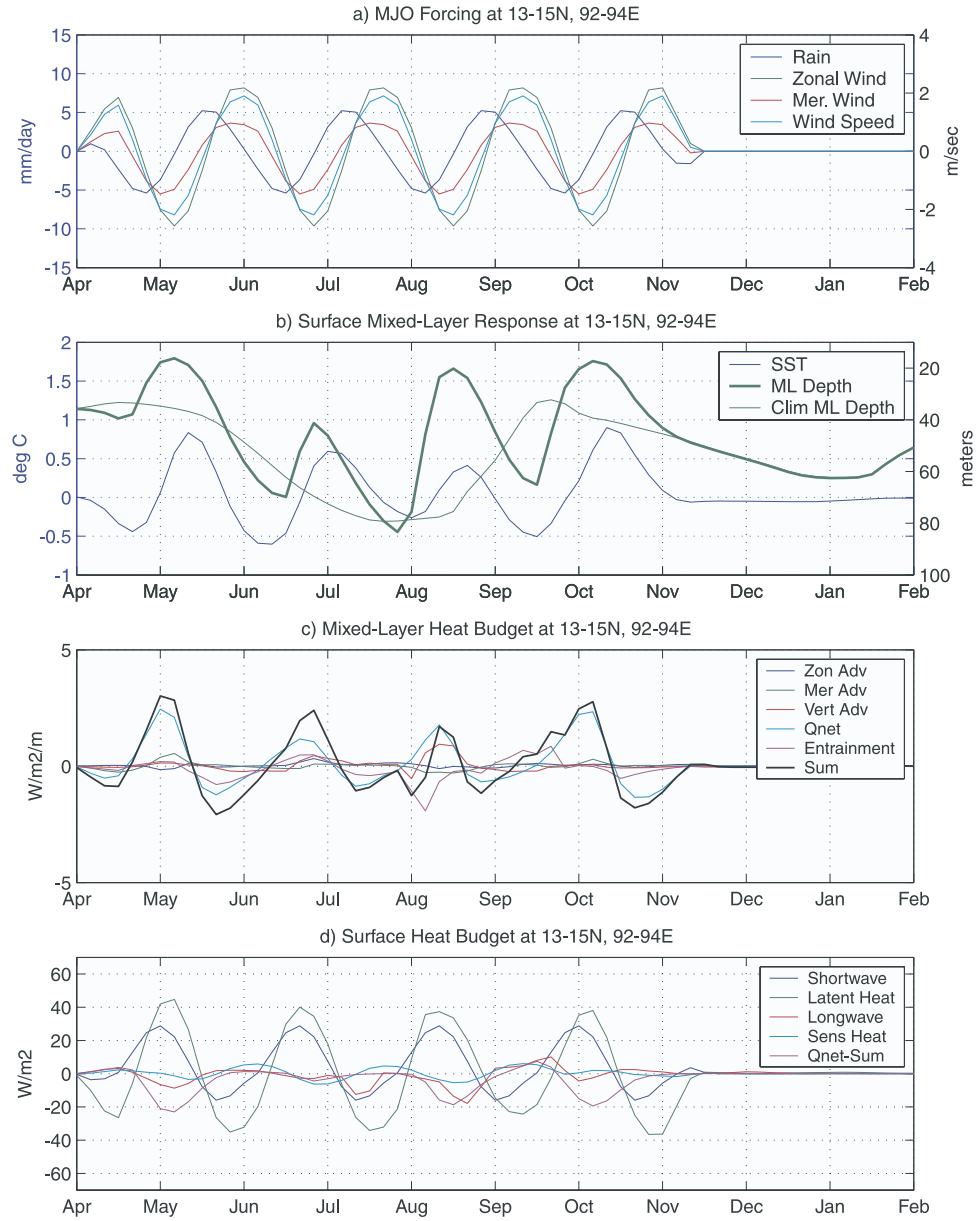

Figure 14. Time series averaged over a 3° × 3° box at 13°–15°N, 92°–94°E of (a) anomalous (i.e., composite) ISO forcing in terms of surface zonal wind (green), meridional wind (red), wind speed (blue-green), and precipitation (blue). (b) Ocean model response in terms of anomalous SST (blue), total mixed layer depth (thick green) for case using ISO forcing, and climatological total mixed layer depth (thin green). (c) Anomalous values of mixed layer heat budget in terms of zonal (blue), meridional (green), and vertical (red) advection, net surface heat flux, which accounts for solar penetration through the bottom of the mixed layer (aqua), entrainment (purple), and the sum of the above terms (black). (d) Anomalous values of surface heat budget in terms of net surface shortwave (blue) and longwave (red) radiation, latent (green) and sensible (aqua) heat flux, and the difference between the actual net surface heat flux that impacted the mixed layer and the sum of the above four terms (purple). This latter quantity is simply the shortwave energy that passed through the bottom of the mixed layer. In the above description, "anomalous" is taken to be the difference between the climatological simulation and the simulation forced with composite ISO conditions.

and during its transition to a cooler but less saline (i.e., enhanced rainfall) mixed layer, is highly effective at shutting down the entrainment that occurs in the climatological simulation (i.e., Figure 16). Thus the positive anomalies in entrainment in Figure 17 during late August and early September do not represent warming by entrainment rather they represent less cooling than that which occurs in the climatologically forced case. Since the magnitude of these entrainment variations are quite large, they account for the relatively large variances exhibited in Figure 9 in the BoB.

[26] Figure 18 shows details of the near surface response for the central equatorial Pacific Ocean, a region that

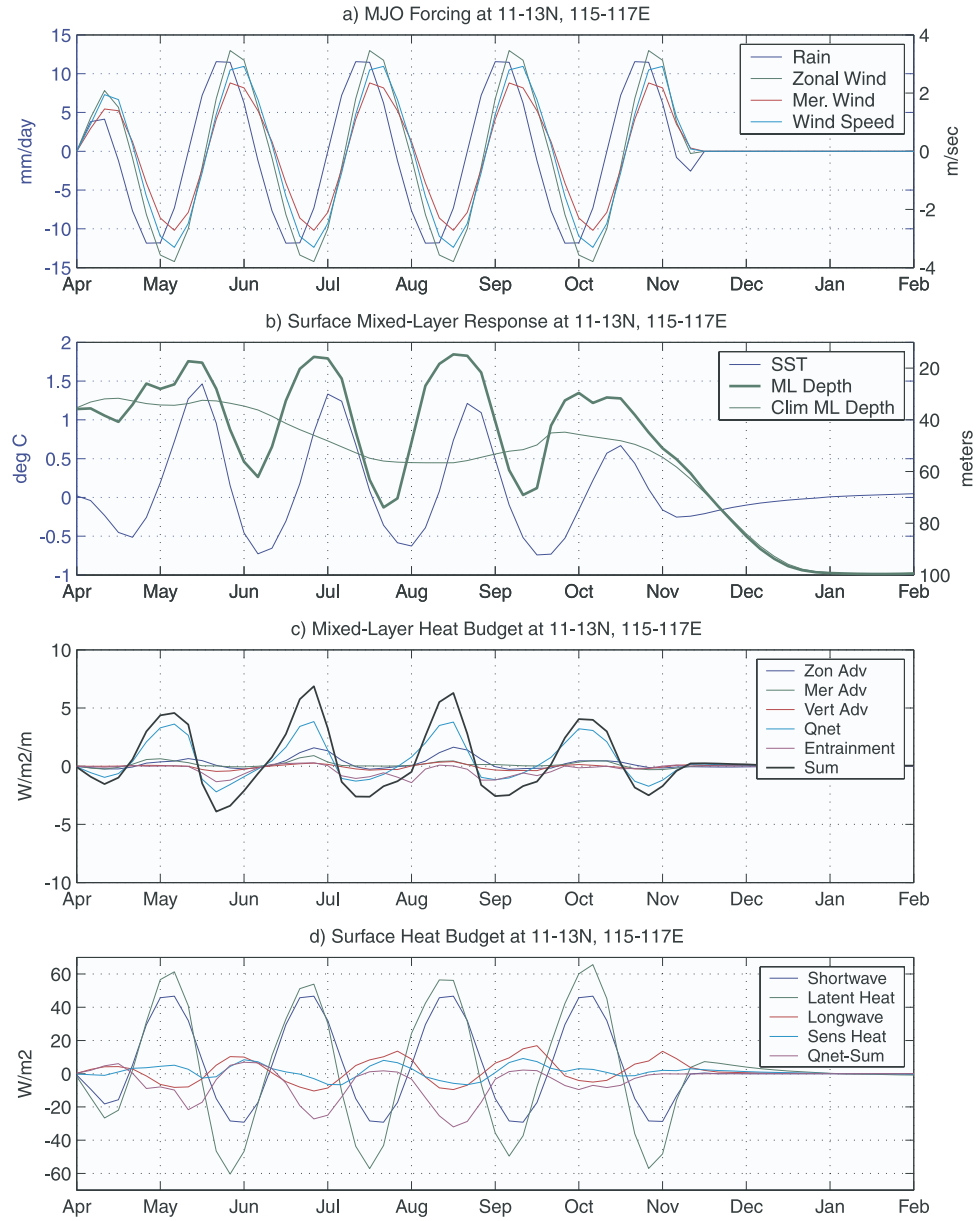

Figure 15. Same as Figure 14, except averaged over the domain 11°–13°N and 115°–117°E.

exhibits relatively low amplitude ISO forcing, and only modest SST variability but rather large MLD variability. Evident from Figure 18a is the rather weak wind forcing ($\sim$1 m^{-1}) and that the anomalous wind speed variations are directly out of phase with the anomalous zonal winds because of the presence of mean easterly trade winds. This in conjunction with virtually no rainfall variability accounts for the weak perturbations in the anomalous surface heat fluxes that are only half or less of the values associated with regions discussed above. In this case, the surface heat flux budget is dominated by the latent heat flux, having variations on the order of ±20 Wm^{-2}. Note that under these composite ISO conditions, the surface shortwave has a net warming contribution over the ISO time period. This issue was raised in section 3.2 and will be discussed in more detail in the next section. While the mixed layer exhibits very small SST variability on the ISO timescale, it does exhibit rather large MLD variations. These arise in this region for this model and its forcing for a number of reasons. First, in general this region is not strongly stratified. This relatively weak (tropical) stratification, coupled with the modest variations in latent heat flux and zonal wind stress lead to relatively large variations in MLD, variations that because of the weak stratification and modest heating, produce only small variations in SST. The zonal wind stress, which exhibits a modest local maximum in this region in the composite (see Figure 6), enhances the MLD variability in two ways. First, it induces a relative maximum in east-west near-surface shear variability at the base of the mixed layer. Second, through wind stirring, it generates turbulent kinetic energy. Each of these processes is specifically accounted for in the hybrid mixed layer model [*Chen et al.*, 1994] and enhance MLD variations.

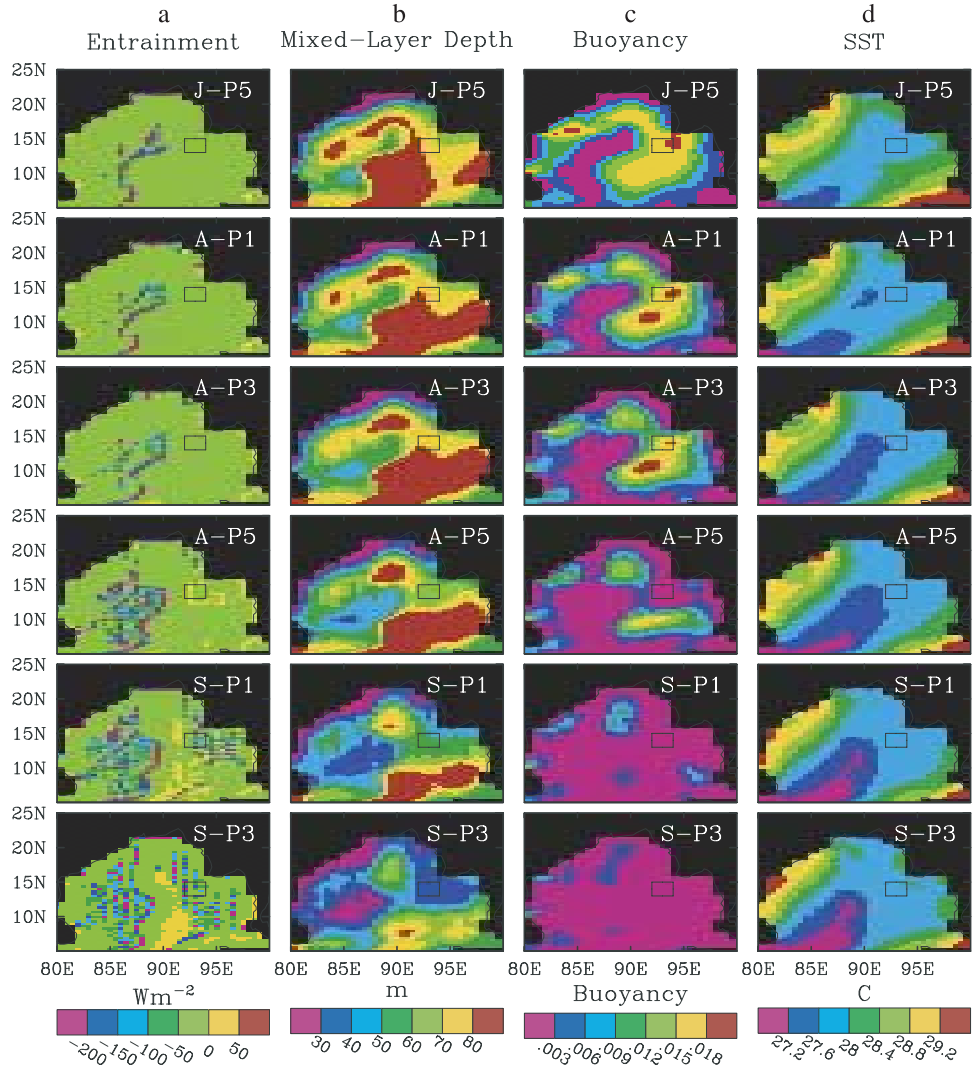

Figure 16. Evolution of (a) mixed layer entrainment, (b) mixed layer depth, (c) buoyancy, and (d) SST from the model climatology for the Bay of Bengal. The time period is indicated by the annotation in the upper right-hand corner of each plot, where J, A, and S indicate July, August, and September, respectively, and PN indicates the pentad number within the month, where N = 1–6. Thus each map is associated with a 5-day average, and the maps are separated by 10 days. The rectangle on each map indicates the region associated with Figure 14. Note that negative values of entrainment imply a cooling of the SST. Buoyancy is defined here as the difference in b between the mixed layer and the layer just below, where b for a given layer is defined as $g(\rho_o - \rho)/\rho_o$ and $\rho_o = 1027.12$ kg m^{-1}.

[27] The region of relatively high MLD variability that occurs near 20°N and 160°E arises from processes fairly similar to the subtropical response discussed by WML. Figure 6 shows that concomitant with the MLD variability in this region is a fair amount of wind (stress) variability with relatively little variability from clouds and rainfall. While this region does not exhibit much SST variability, it is instructive to briefly illustrate the relevant processes that influence this MLD variability. Plots such as Figure 14 for this region (not shown), along with other analysis, show that climatologically the mixed layer is relatively deep (~70 m in boreal summer, increasing to 100 m in austral summer) and the water column exhibits relatively weak stratification given the somewhat cooler subtropical surface waters. The intraseasonal wind speed forcing varies between approximately ±1.5 m s^{-1} and leads to latent heat fluctuations of about 20 Wm^{-2}, which completely dominate the surface heat flux budget. This wind-induced surface heat flux forcing, and associated influence on the production of turbulent kinetic energy, leads to MLDs on the order of 40–60 m (80–90 m) under the low (high) wind speed phase of the ISO forcing. While this MLD change is relatively large, the fact that it arises in conjunction with weak stratification, rather small net surface heat flux anomalies, and relatively large total MLD, implies that there will be very little impact on the SST (~±0.2°C).

[28] Finally, a note about the variability observed in the region of the Somali current. While there is a modest

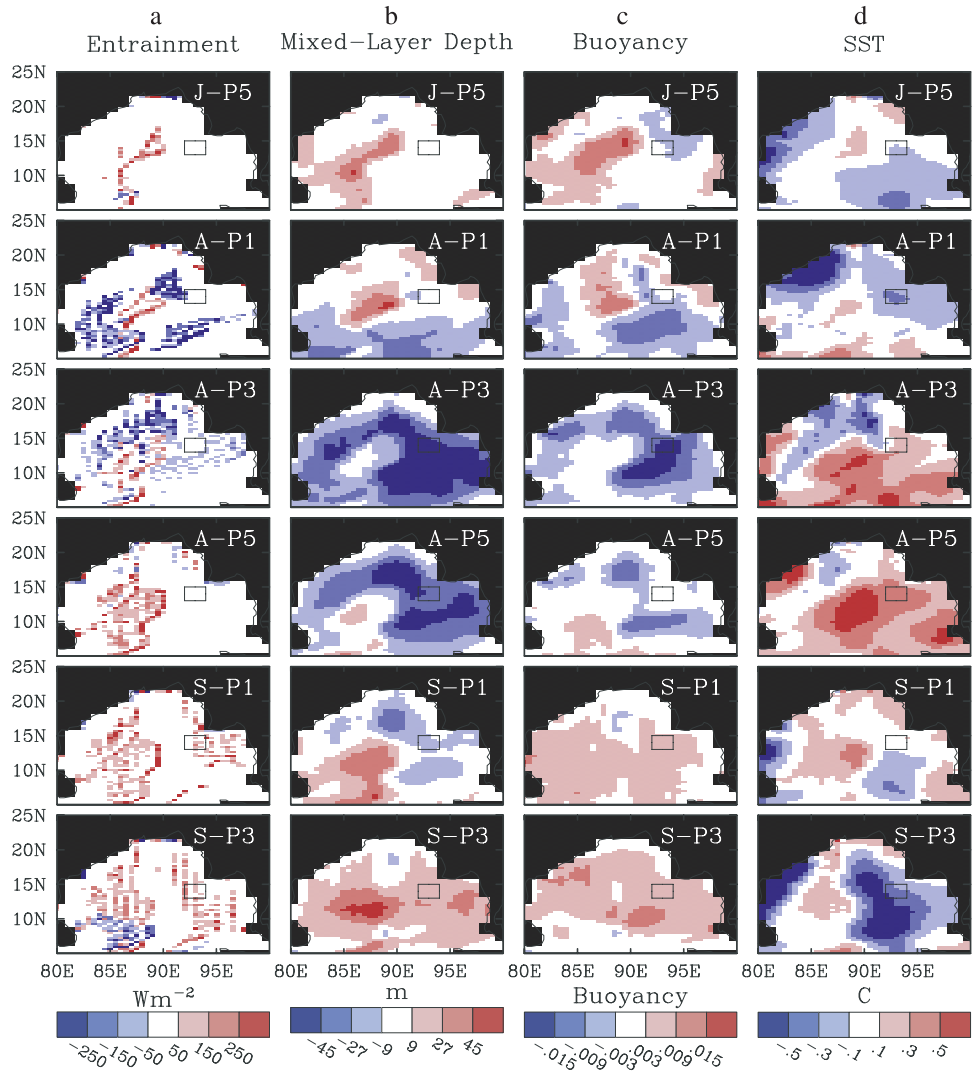

Figure 17. Same as Figure 16, except for the difference between the simulation with ISO forcing and the climatological forcing.

amount of intraseasonal variability in SST (Figure 8) and a considerable amount of intraseasonal variability associated with advection (Figure 9), these terms show very little systematic relationship to the repeating cycle of the ISO forcing (Figure 4). In terms of the forcing itself, the cloud/shortwave and rainfall components are quite weak (Figure 6), although there is about a 1.5 m s^{-1} peak-to-peak variation in the wind components, with the zonal and meridional components tending to vary in phase. However, these (weak) wind variations do not translate into robust/systematic variations in latent heat flux because of the dependence of the latent heat flux formulation on the evolving SST itself (which in this region is not dominated by surface heat flux variations) and because of its dependence on the offshore wind pattern and land-sea boundary values of humidity. While the vertical advection does exhibit the expected relationship with the wind forcing (with a magnitude of about ±0.5 W m^{-3}), it is often overwhelmed by what appears to be more transient variability in zonal and meridional advection that stems from coastal Kelvin wave activity. In addition to the above, the SST response is also nonuniform over the ISO forcing period because of the evolving state of the MLD, which deepens from about 40 m in April to over 100 m in June and then shoals back to around 40 m during September.

4.3. Sea Level and Transports

[29] As mentioned earlier, relatively large sea level variations occur on the eastern side of both ocean basins (Figure 8). This, in conjunction with the zonal current composite (Figure 13) and sea level composite (not shown) indicate that this activity stems from equatorial Kelvin waves. Figure 19 demonstrates the nature of this sea level activity for the eastern Indian Ocean. The thick line with circles shows the main element of the forcing, i.e., the surface zonal wind, in the central equatorial Indian Ocean (marked as X on map). The rainfall variations associated with the ISO wind perturbations are also shown in order to identify the region of strongest convection. The sequence of heavy dashed/dotted lines shows the sea level perturbations at a number of locations, starting off the West Coast of Sumatra and moving north around to the western coast of

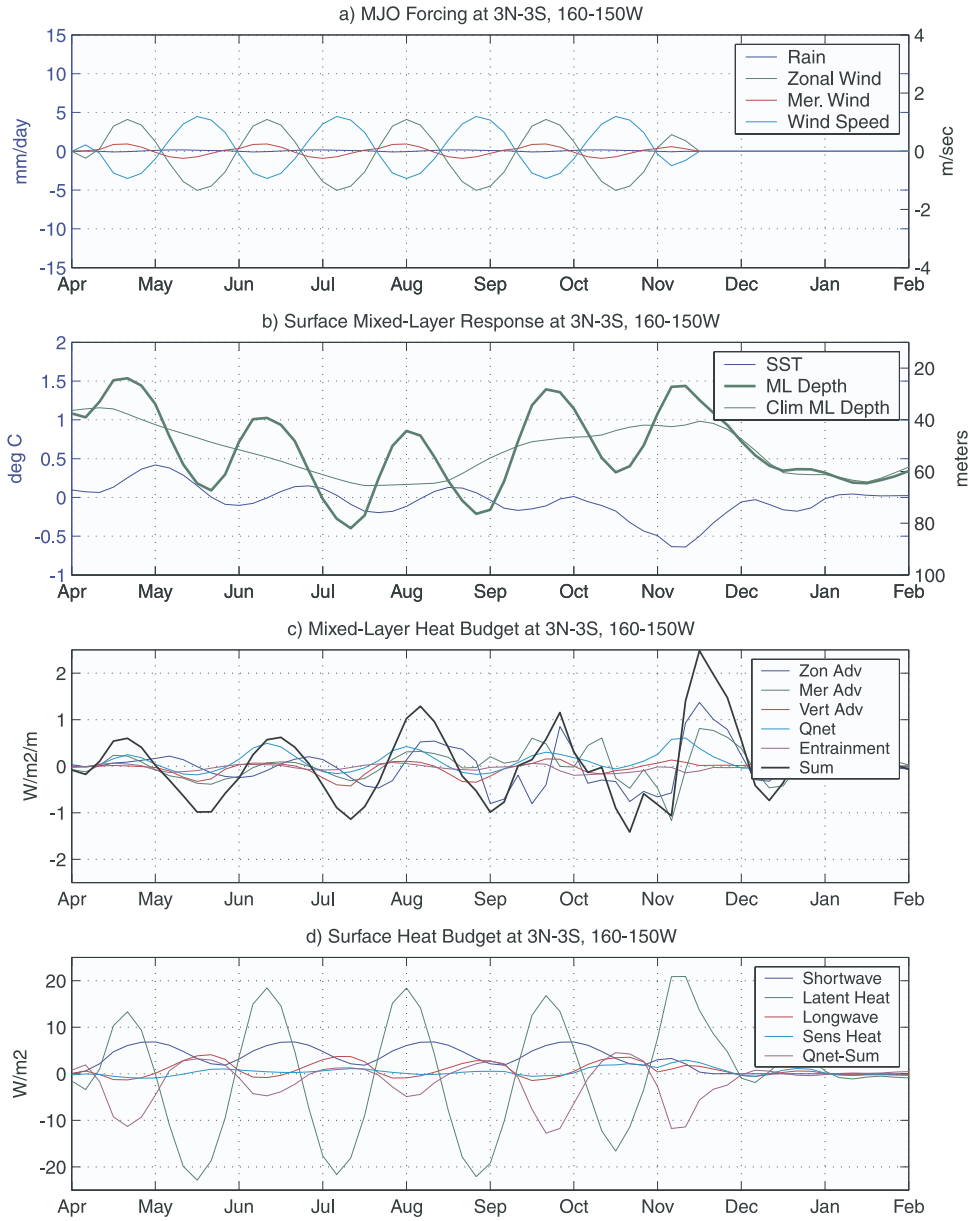

Figure 18. Same as Figure 14, except averaged over the domain 3°N–3°S and 160°–150°W.

the BoB and including one point to the south on the southern coast of Java. The plot shows that positive sea level anomalies on the order of 5–8 cm would be expected to occur at the Sumatra (western BoB) location about 25 (50) days after a positive ISO precipitation anomaly occurs in the central Indian Ocean, with a similar lag relationship holding for negative anomalies. Remote forcing of the seasonal and interannual variability of coastal sea levels in the BoB has been noted before [e.g., *Potemra et al.*, 1991; *Clarke and Liu*, 1994; *Han and Webster*, 2002] but our results indicate that similar wave dynamics are also likely at work at ISO timescales. This is important for remote forcing of the Indonesian Throughflow (ITF) and coastal upwelling off Java and may affect interannual variability at basin scales [*Sprintall et al.*, 2000; *Annamalai et al.*, 2003]. The sea level activity at the eastern side of the Pacific basin is analogous to that found in the Indian Ocean basin, although the zonal scale of the Kelvin waves in the Pacific Ocean is on the order of 4000 km while the zonal scale in the Indian Ocean is only about 1000 km.

[30] Associated with the sea level and current variations discussed above are variations in basin-wide transports. As with WML, only the ITF and the cross-equatorial Indian Ocean transports will be highlighted. Figure 20 shows the model heat (and mass, see caption) transports associated with the applied canonical ISO forcing. In Figures 20a, 20b, 20e, and 20f the results are put into the context of the climatology, while Figures 20c, 20d, 20g, and 20h simply show the anomalies. Rather remarkable in the case of the ITF (Figures 20a–20d) is that the magnitude of the intraseasonal variability (±∼1 PW) forced by the ISO is at least as large as the annual cycle, and equally as large as

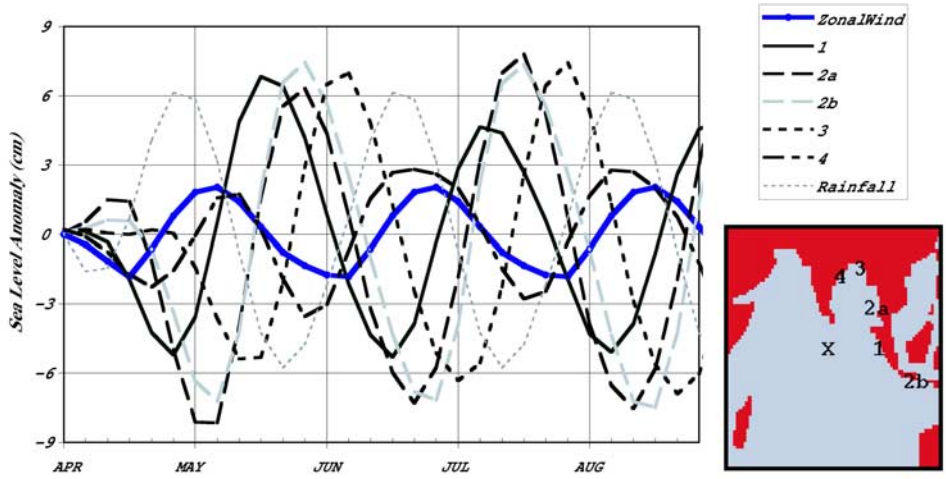

Figure 19. Composite ISO forcing in terms of surface zonal wind (thick solid; same scale in m s^{-1}) and rainfall (thin dotted; same scale mm d^{-1}) in the central equatorial Indian Ocean (shown as a cross in map). Anomalous ocean model sea level response (solid, dashed, shaded dashed, short-dashed, and dot-dashed) at a number of coastal locations in the eastern Indian Ocean (shown as 1, 2a, 2b, 3, and 4 in map).

estimates of interannual variability in the ITF [*Murtugudde et al.*, 1998]. This result is nearly identical to what was found for the austral summer case examined by WML (see their Figure 17). The main difference is that the ISO perturbations occur when the climatological ITF transport is most negative, and even though the intraseasonal perturbations in ITF transport are nearly the same size as for the austral summer case, the total ITF value for the boreal summer case never becomes positive as it does for the austral summer case.

[31] In contrast to the ITF, and similar to the findings of WML, the relative sizes of the climatological and anomalous cross-equatorial Indian Ocean transport have the opposite relation. The annual cycle of the north-south heat transport, which has been hypothesized to play an important role in the coupled ocean-atmosphere regulating system of the Asian monsoon [*Loschnigg and Webster*, 2000], has an amplitude of about ±2PW. On the other hand, the range of the intraseasonal variations is only about ±0.3 PW. While these variations extend deeper (∼150 m) than for the austral summer case (∼100 m; see Figure 17 of WML), they are rather weak relative to the ITF. This is due to the orientation of the wind variability (i.e., mostly zonal), the fact that the anomalies do not penetrate as deep (∼<100 m), and there is a strong baroclinic nature that leaves only relatively small residual values. Further discussion of the climatic implications of the above sorts of findings is given by WML and will not be repeated here.

4.4. Rectification to Low Frequencies

[32] A significant amount of attention was paid by WML to the issue of the rectification of the intraseasonal timescale of the ocean response onto lower frequencies. The full depth of that discussion and analysis will not be repeated here since much of the discussion, results and associated mechanisms are independent of season. The main emphasis here will be to highlight features and processes associated with rectification that are new or that appear to exhibit a seasonal dependence. By way of a brief introduction, it should be pointed out that apart from the intraseasonal fluctuations shown in Figures 12, 14, and 15, there is also a rectification of the intraseasonal model response onto lower frequencies. For example for each of these figures, the mean MLD over the period of the active ISO forcing is less than for the model's climatological MLD. Similar low-frequency variations occur in the SST. As discussed below, part of this rectification arises from the fact that the composite forcing contains nonzero residual mean values that were discussed in section 3.2 (e.g., see composite ISO shortwave time series in Figures 15 and 18) and part arises because of nonlinearities in the near surface ocean response. These low-frequency characteristics are more evident in the maps of the mean anomalous response shown in Figure 21. The latter illustrates that the application of the control case ISO forcing to the ocean model leads to a slight warming (∼0.2°C) in the northern Indian and northwestern Tropical Pacific oceans during the period of active ISO forcing. Concomitant with this low-frequency warming is a mixed layer shoaling of about 10–15 m. In addition, the equatorial Indian (western Pacific) exhibits a mean eastward (westward) current bias of about 5–10 cm s^{-1}.

[33] To examine the degree to which the rectification discussed above stems from ocean rectification processes versus a rectified signal in the ISO forcing itself, it is important to reiterate that the method used for compositing did not require the forcing associated with the "anomalous" ISO cycle to have zero mean (albeit the "residual" means were small). Rather, the intention was to simply try to capture an accurate depiction of an ISO event, with specific effort made to limit biasing of the forcing that might arise from interannual variability (i.e., via band-passing). To determine the influence that these residual means have on the rectified signal, a simulation was carried out in which the residual means were removed from the composite ISO forcing components (i.e., solar, winds, clouds, and rain). The results of this experiment are shown in Figure 21b. Similar to WML, much of the rectified signal in SST disappears, much of the MLD signal remains, and the zonal

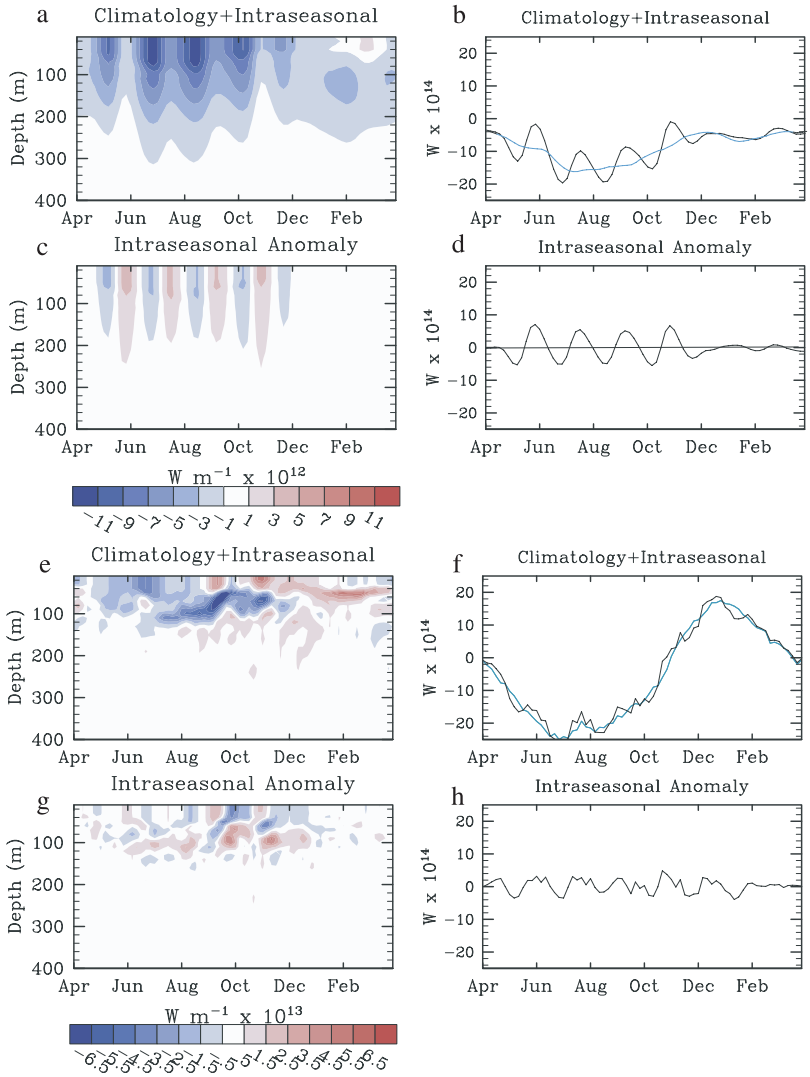

Figure 20. (a) Total zonal heat transport across 114°E as a function of time and depth for the simulation using ISO forcing. (b) Depth-integrated ($z < 400$ m) heat transport across 114°E as a function of time. The smooth line is the climatological value. (c) and (d) Same as Figures 20a and 20b, except showing the differences between the case with and without (i.e., climatology) ISO forcing. (e)–(h) Same Figures 20a–20d, except for cross-equatorial transport in the Indian Ocean. Note the scale change. Mass transport plots (not shown) look very similar except that the units and scales for the color bars are $m^2\ s^{-1} \times 10^4$ (10^5) for Figures 20a–20d (20e–20h) and units and scales for the line plots are $m^3\ s^{-1} \times 10^6$.

current signal appears to simply weaken. This result suggests that most of the SST rectification is associated with a rectification of the ISO forcing itself, most of the MLD rectification is associated with nonlinear mixed layer processes, while the rectification of the zonal current contains elements of both.

[34] Additional sensitivity runs that excluded various components of the perturbation forcing are helpful in further understanding the nature of the rectification that occurs in the control case (Figure 21a). It was found that most of the rectified signal associated with SST is derived from low-frequency rectification of the shortwave component of the ISO forcing. For example, the results in Figure 21b show that when the residual mean of the ISO shortwave perturbation forcing is excluded, then not only does most of the net warming disappear but parts of the northwest Pacific exhibit a net cooling. However, for this case, neither the MLD nor zonal current rectification is substantially impacted. The results of this simulation strongly suggest that the small, positive residual mean shortwave anomalies associated with an ISO event (which, as constructed in this study, range between 3–5 Wm^{-2} over most of the Indo-Pacific basin but are as large as 10 Wm^{-2} in the northwest Tropical Pacific and South China Sea region) can produce small positive SST anomalies over the course of an ISO event. This is likely to be related to the fact that for an ISO (or MJO) event, the area of convection is smaller than the ISO-induced areas of subsidence, thus over the course of an ISO event more time is spent under suppressed cloud conditions [*Myers and Waliser*, 2003].

[35] No aspect of the ISO forcing in particular was found to be responsible for the bulk of the mean MLD shoaling

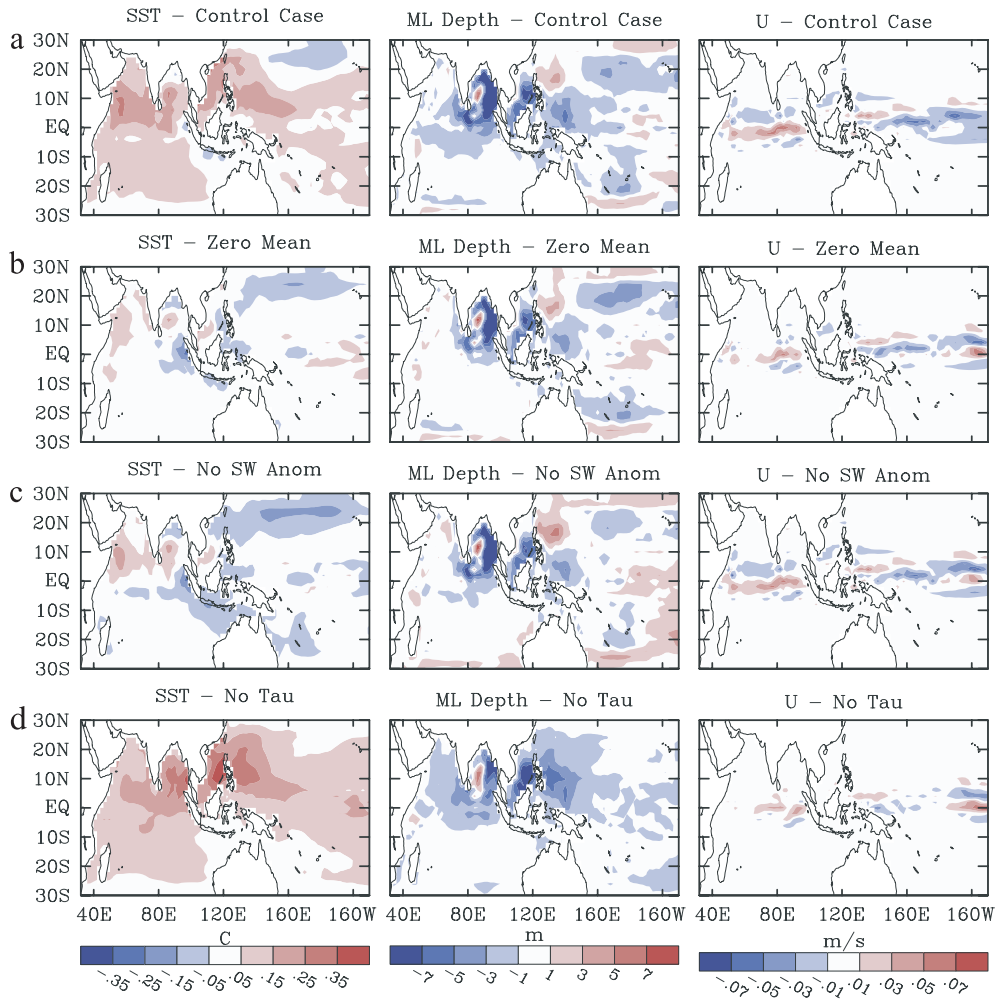

Figure 21. Time mean maps of anomalous ocean response (i.e., difference between ISO case and climatological case) in terms of (left) SST, (middle) mixed layer depth, and (right) surface zonal current associated with (a) ISO forcing for the control case; (b) as in the control case, except with the residual means of the ISO forcing structure removed; (c) as in the control case, except with the residual means of only the ISO shortwave forcing structure removed; and (d) and as in the control case but with no ISO wind stress forcing. Time averages were taken over the four complete ISO cycles, i.e., pentads 4–43 (see section 3 and Figure 4).

that occurs in the control case. Thus, as discussed by WML, the MLD shoaling appears to be associated with the basic nonlinear aspect of the mixed layer that a given positive anomaly in heating is typically more effective at shoaling the MLD than a negative anomaly is at deepening it [*Kraus and Turner*, 1967]. This effect will of course be accentuated if the wind mixing anomalies (i.e., anomalies in mixed layer TKE generation) tend to be in phase with the net surface heat flux, so that surface heating anomalies also occurred during times of reduced wind mixing; this is typically the case with an ISO event (see Figures 14, 15, and 18). In regards to the rectification of the zonal current, results in Figure 21d, not surprisingly, show that the rectification stems from interactions with the wind stress forcing. The nature of the rectification that occurs in the western Pacific was discussed in some detail by WML and, in short, was found to be associated with the fact that the MLD shoals during the easterly wind phase and deepens during the western. The anomalously deep mixed layer does not accelerate as readily as the shallow layer, resulting in a net westward bias to the surface current.

[36] The austral summer case treated by WML exhibited no zonal current rectification in the Indian Ocean, however in the boreal summer control case treated here, there is a net eastward bias. Examining the results from a simulation that excluded the mean residual bias in the wind stress forcing shows that some component of this zonal current bias stems from the fact that the westerly stress anomalies are slightly bigger than the easterly stress anomalies along the central equatorial Indian Ocean (not shown). However, even then there is a net eastward bias in the zonal current along the equator, mainly confined in that case to the eastern part of the basin (east of 80°E). Analysis to determine the cause of this component of the current rectification was inconclusive. However, it should be noted that the mean zonal current is varying over the period of the anomalous forcing. For example, the first positive zonal wind anomaly produces a strong anomalous eastward current (~25 cm s^{-1}) that

corresponds exactly to the period when the model's Wyrtki jet [*Wyrtki*, 1973] is strongest ($\sim$35 cm s^{-1}). Similarly, the final event occurs during the (weaker) fall Wyrtki jet ($\sim$25 cm s^{-1}). Moreover, time-longitude plots (like that of Figure 18 of WML) indicate that the model's anomalous current response is stronger during the period of increased jet strength. Thus there is also the possibility that there might be nonlinear interactions between these anomalous and mean currents that may lead to one, relatively small, component of zonal current rectification seen in Figure 21. This issue needs to be examined in more detail and to examine the sensitivity of the (fall and spring) Wyrtki jet to the amplitude and phase of the imposed ISO forcing. In addition to the effects of the wind stress forcing on zonal current, it is worth noting that when the ISO-related wind stress forcing is excluded (Figure 21d), the rectified signal in SST and MLD become larger. This is associated with the fact that while stress is related to the square of the wind speed, TKE generation is related to the cube of the wind speed (i.e., the work generated). Adding an anomalous oscillating wind stress component (i.e., the control case) to a background wind stress results in the generation of more wind-mixed TKE in the mixed layer and thus a likely decrease (increase) of the SST (MLD); thus by excluding this anomalous component (i.e., Figure 21d) the SST (MLD) would tend to increase (decrease).

5. Summary

[37] The objective of this study was to examine the basin-wide response of the Indo-Pacific Oceans to atmospheric forcing associated with the Intraseasonal Oscillation (ISO). The purpose was to obtain a comprehensive view of the ocean variability that might be directly attributed to the ISO and to examine the mechanisms underlying this variability. In doing so, our intention was to broaden the perspective offered by previous studies whose findings were necessarily limited because of observational constraints, simplified model physics, and/or regional dependencies [e.g., *McCreary et al.*, 1993; *Bhat*, 2001; *Han et al.*, 2001; *Sengupta et al.*, 2001a; *Sengupta and Ravichandran*, 2001; *Sengupta et al.*, 2001b; *Vecchi and Harrison*, 2002; *Webster et al.*, 2002]. Because of the relative abundance of atmospheric (forcing) data and the relative paucity of ocean (response) data, an ocean GCM framework with imposed forcing was utilized. Significant care was taken to develop canonical forms of ISO forcing from the available observations (Figures 2–6) and then to use them with an ocean GCM that demonstrates reasonable fidelity in representing the ocean response to ISO forcing (Figure 9) [see also *Shinoda and Hendon*, 2001]. The primary issues addressed in this study involved determining: 1) the general scope of tropical ocean variability that could be attributed to typical ISO forcing (e.g., regional dependence, strength of response, and local versus remote), 2) the particular components of the forcing that were the most important; and 3) the relative contributions of the different physical mechanisms responsible for the ocean response. In this study the response was measured in terms of physical properties, such as circulation, temperature, mixed layer depth (MLD), salinity and sea level variations. In addition, a number of more specific issues were examined, such as the effect on basin-scale transports, remote effects via wave propagation, rectification of the intraseasonal timescale to lower frequencies, and the degree to which 3-D ocean physics are required to represent the ocean's temperature response.

[38] The results show that the imposed ISO forcing induces ocean variability that both is local to the region of intense convective activity (i.e., northern Indian and northwestern tropical Pacific Oceans) and has considerable variability outside this region (Figures 8, 9, 12, and 13). The former consists of variations, measured in terms of standard deviation, that range up to about 0.6°C in SST, 20 m in MLD, 0.2 m s^{-1} in surface current, 5 cm in sea level, and 0.1 psu in salinity. While some aspects of the near-surface ocean variability associated with the ISO has been documented [e.g., *Bhat*, 2001; *Kemball-Cook and Wang*, 2001; *Sengupta et al.*, 2001a; *Sengupta and Ravichandran*, 2001; *Vecchi and Harrison*, 2002; *Webster et al.*, 2002], obtaining a basin-scale perspective of this variability has not been forthcoming, particularly for MLD and surface currents. Moreover, the magnitude and large-scale nature of the SST variations produced by the ISO forcing are bound to have important ramifications on the evolution and nature of the rainfall anomalies associated with the Asian summer monsoon [*Annamalai and Slingo*, 2001; *Kemball-Cook and Wang*, 2001; *Sengupta et al.*, 2001a; *Kemball-Cook et al.*, 2002; *Vecchi and Harrison*, 2002; *Wu et al.*, 2002; Y. Zheng et al., The role of coupled sea surface temperatures in the simulation of the tropical intraseasonal oscillation, submitted to *Climate Dynamics*, 2003]. The findings in this study, based on the OGCM, suggest that in most areas of the northern Indian and northwestern tropical Pacific Oceans, the SST variations are driven to a large extent by the net surface heat flux variations (Figures 14 and 15). Consistent with earlier studies and expectations, the main contributing forcing components in these cases are wind speed via its effects on evaporation, and cloudiness via its effect on shortwave (Figure 10). Other components of the forcing, such as rainfall, and cloud cover effects on longwave, in general, make much less contribution to the SST variability. In terms of magnitude and phase, variations in shortwave and latent heat flux are considerable and tend to act in phase to heat/cool the SST, variations in longwave are modest but tend to be out of phase with the shortwave, and variations in sensible heat flux are negligible. In the areas most strongly and directly affected by ISO forcing (e.g., northern Indian and northwestern tropical Pacific Ocean), MLD variations were also found to be considerable (e.g., Figures 8 and 12) and important in determining the SST variability. For the most part, these variations contributed in a positive manner to the SST variations since the heating/cooling variations were imparted on a shallower mixed layer. However, in some cases this shoaling became so significant ($\sim$20–30 m) in the context of the background MLD ($\sim$40–60 m) that nontrivial amounts of solar radiation penetrated through the bottom of the mixed layer [e.g., *Anderson et al.*, 1996; *Sengupta and Ravichandran*, 2001]. However, it is should be stressed that while the variations exhibited in MLD by the model are in rough agreement with the few observations available, basin-wide intraseasonal MLD variability is a quantity that sorely needs to be better observed and documented.

[39] Aside from the general conclusions discussed above, there are a number of places where variations in entrainment

and three-dimensional ocean advection do make nontrivial contributions to the mixed layer heat budget (e.g., Figure 9). In particular this includes a significant amount of entrainment variability in the Bay of Bengal, modest contributions from advection and entrainment in the South China Sea, and large contributions from advection and entrainment along the equator in the Indian and eastern Pacific Oceans. In regards to the latter, much of the SST variability derives from entrainment and advection; the details of which appear to be somewhat insensitive to season and are discussed by WML. One noteworthy difference between the austral and boreal summer cases is that there were no large-scale ocean regions that exhibited large values of entrainment variability in the austral summer case as there are for the boreal summer case, namely the large entrainment variability exhibited in and south of the Bay of Bengal. During the warm SST phase of ISO, the normally large climatological values of the entrainment in this region (Figures 16 and 17) are effectively shut down. This along with the modest increases in entrainment during the disturbed phases of the ISO lead to these large entrainment variations on intraseasonal timescales. We plan to examine this issue in even more detail in our future research, including how the phase of the ISOs relative to the annual cycle might play a role in this entrainment variability, and in the establishment and breakdown of any barrier layer that might develop in the Bay of Bengal. In contrast to most of the regions discussed above and by WML, in which surface heat flux plays either a dominating or important role, the modest SST variability that develops off the Somali coast in association with the ISO forcing is mostly derived from ocean dynamics with very little is derived from air-sea heat fluxes. While the ISO does have some effect on the wind variability in this region, it produces little or no modulation of cloudiness/convection, and thus of surface shortwave radiation, which in most of the cases described above plays a significant, and often the most significant, role in the determining the size of the air-sea heat flux variations.

[40] Apart from the Indo-Pacific areas discussed above, the ISO-related intraseasonal variability in a number of other, more remote, regions was also examined. This included the remotely forced SST variability in the equatorial eastern Pacific that was found to be generally analogous to the eastern Pacific variability treated by WML. In addition, it was noted that considerable MLD variability occurred in the central equatorial Pacific Ocean. This variability was determined to be associated with modest local wind forcing variability and weak vertical stratification which when considered together gives rise to MLD variations via both thermodynamic (e.g., buoyancy) and dynamical mechanisms (e.g., stirring and shear). Finally, analogous to the results of WML for the wintertime subtropics, there are also large MLD variations in the summer subtropics (i.e., Northern Hemisphere subtropics in this case). The size of these MLD variations are of the same order as for those regions discussed above where the forcing is considerably larger (e.g., Bay of Bengal and South China Sea) but in contrast to those regions there is very little impact on the SST (e.g., Figures 6 and 8). Despite the weak local forcing, the large magnitude of the MLD variations in the subtropics stems from the relatively weak vertical stratification. As with the austral summer analysis of WML, this weak stratification and surface flux forcing, in addition to the relatively large climatological MLDs there, strongly limit the size of the SST variations.

[41] In conjunction with ISO wind stress forcing are remotely forced sea level variations, via Kelvin waves, on the equator and the eastern sides of the Indian and Pacific Ocean basins (Figure 8). In the case of the Indian Ocean, these variations are on the order of 5–10 cm and travel for example from the central part of the basin well into the Bay of Bengal (Figure 19) and down the southern coast of Java and into the Indonesian seas. While such variability has been noted before in conjunction with seasonal and interannual variability, these results show that the same sort of Kelvin wave driven variability occurs on ISO timescales as well. In particular, for a positive ISO-induced rainfall anomaly occurring in the central Indian Ocean, a positive zonal wind stress anomaly typically develops about 2 weeks later. Subsequently, sea level is found to rise at the eastern side of the basin (i.e., Sumatra) about 1 week later, and found to rise in the Bay of Bengal about 3–4 weeks later (i.e., 6 weeks after the central Indian Ocean rainfall event). In conjunction with these sea level variations are variations in basin-wide transports (Figure 20). For example, variations in the ITF brought about by ISO wind stress forcing are of the same order of magnitude as the seasonal cycle of ITF transport ($\sim$1 PW; 10 Sv). In contrast, the variations associated with the climatological cross-equatorial flow in the Indian Ocean basin are considerably larger ($\sim\pm$2 PW) than those associated with ISO forcing ($\sim\pm$0.3 PW). It is worth noting that the relatively small amplitude of the model's intraseasonal oscillations in cross-equatorial compared to the annual cycle contradicts the findings of *Loschnigg and Webster* [2000]. In their model study, the magnitude of the annual cycle of cross-equatorial transport was similar to that found in the present study but the amplitude of the intraseasonal fluctuations was about a factor of 5–10 larger than that exhibited here. It is likely that their model's crude vertical resolution (i.e., 2.5 layers for the upper ocean) does not exhibit the rather complex baroclinic variations that are simulated in the model described here (i.e., Figures 20e and 20g), which could lead to an overestimate of these variations in transport, at least relative to those simulated by the model used in this study.

[42] Considerations were made to address whether and how the intraseasonal timescale of the ISO forcing might lead to longer timescales of variability in the ocean (Figure 21). This rectification issue was first examined by *Kessler and Kleeman* [2000] where idealized MJO wind forcing was applied to virtually the same ocean model that is used here. Significant attention was paid to this issue by WML in regards to the austral summer case and the MJO. Similar to that study, the imparted ISO forcing produced a net low frequency (i.e., average anomalous response of the ocean model to the imposed ISO forcing) SST warming ($\sim$0.1°C) and MLD shoaling ($\sim$7 m) over much of the northern Indian and northwestern tropical Pacific Oceans. The rectified SST signal was found to be mostly associated with a rectified (i.e., residual mean) signal in the shortwave forcing (see section 3.2), meaning the composite ISO contains more periods/regions of suppressed convection than enhanced convection which is not unreasonable given the nature of convective organization [see also *Myers and*

Waliser, 2003]. The MLD shoaling appears to result from nonlinear mixed layer processes rather than from any residual means associated with the forcing, namely, that a given size positive surface heat flux anomaly is more effective at shoaling the mixed layer than a negative one is at deepening it. The imposed ISO forcing was found to induce some modest low-frequency rectification in the equatorial zonal current, in part attributed to the rectified signal in the wind stress forcing itself and possibly because of an interaction between the anomalous currents and the evolving state of the background zonal current (e.g., spring and fall Wyrtki jet). Apart from the other ISO forcing components, the ISO wind stress forcing was also shown to independently lead to a cooler (deeper) SST (MLD) by about 0.1°C (2 m) over the regions where the direct forcing is greatest.

[43] In regards to the above findings on the low-frequency rectification of the ISO timescale, it should be stressed that additional experimentation is needed using other forcing scenarios and other ocean GCMs to more clearly separate aspects associated with rectification of the forcing as opposed to rectification that occurs via ocean processes. In addition, for future studies, it is worth considering the rectification issue in the context of the following question: Does a season with strong ISO activity have a different ''background state'' than one with weak activity? If there were a systematic difference in the means between these two types of seasons, then it is worthwhile considering how to categorize this (low-frequency) variability. For example, a number of studies, along with this one, would seem to indicate that different mean seasonal values would result from years with strong versus weak ISO activity [e.g., *Ferranti et al.*, 1997; *Kessler and Kleeman*, 2000; *Lawrence and Webster*, 2001; *Myers and Waliser*, 2003]. On one hand, it could be argued that the difference in the means could be considered to be an intrinsic change in the background state itself, and that the ISO variability resides above and beyond this change in background state. Thus the difference in the seasonal means between the strong and weak ISO seasons is presumed to be actual/underlying changes in the background itself, a change that might have arisen independent of the difference in ISO activity. On the other hand, it might be that the change in the seasonal mean is actually due to the asymmetries in the ISO phenomena/variability itself (e.g., more clear sky versus cloudy anomaly over a given event or more west versus east wind anomaly, etc). In this case, the background state would be intrinsically considered to be the same for the strong and weak ISO seasons, but a low-frequency rectified signal from the ISOs produces a low-frequency anomaly that rests on top of the ''constant'' background state. However, since the anomaly is of very low frequency, it could be interpreted (i.e., first argument above) as a change to the background state rather than an anomaly on top of the background state.

[44] Both WML and this study have tended to follow the second point of view given above. In assessing which of the two views is more appropriate or meaningful, it is worth considering the following question: Why are there years that exhibit more versus less ISO activity? One possibility is that there is something in the background state that makes this so (e.g., low-frequency SST changes). Thus a changing background state induces changes in the frequency and/or amplitude of ISOs. This possibility is somewhat consistent with the first viewpoint given above, although it doesn't completely preclude effects from the second viewpoint. Thus far, observational and modeling studies [*Gualdi et al.*, 1999; *Hendon et al.*, 1999; *Slingo et al.*, 1999; *Waliser et al.*, 2001] do not suggest a very strong link between interannual SST and interannual changes in ISO activity, although there could well be other aspects to consider in regards to a changing background/boundary condition state. A second possibility is that the frequency and amplitude of ISOs is rather chaotic in nature, somewhat supported by near-null result of the studies mentioned above regarding interannual SST variability. If this is the case and a given ISO event is not symmetric in the sort of anomalies it produces over its life cycle, then the combination of these two would lead to changes in the low-frequency character of a season with strong versus weak ISO activity, and thus in turn lead to a change in the ''background state''.

[45] **Acknowledgments.** Support for this study was provided by the National Atmospheric and Aeronautics Administration under grants NAG5-11033 (DW, LL) and Salinity, QUICKSCAT, TRMM, and Indian Ocean Biogeochemistry grants (RM) as well as the National Science Foundation under grant ATM-0094416 (DW). We would like to thank William Kessler and James Potemra for providing a number of helpful comments and suggestions on Parts I and II of this study. This study's analysis and presentation benefited from the use of the NCAR Graphics Package and Seaspace Corporation's TeraScan software system.

References

Anderson, S. P., R. A. Weller, and R. B. Lukas (1996), Surface buoyancy forcing and the mixed layer of the western Pacific warm pool: Observations and 1D model results, *J. Clim.*, *9*, 3056–3085.

Annamalai, H., and J. M. Slingo (2001), Active/break cycles: Diagnosis of the intraseasonal variability of the Asian summer monsoon, *Clim. Dyn.*, *18*, 85–102.

Annamalai, H., J. M. Slingo, K. R. Sperber, and K. Hodges (1999), The mean evolution and variability of the Asian summer monsoon: Comparison of ECMWF and NCEP-NCAR reanalyses, *Mon. Weather Rev.*, *127*, 1157–1186.

Annamalai, H., R. Murtugudde, J. T. Potemra, S. P. Xie, P. Liu, and B. Wang (2003), Coupled dynamics over the Indian Ocean: Spring initiation of the zonal mode?, *Deep Sea Res.*, *50*, 2305–2330.

Atlas, R., R. N. Hoffman, S. C. Bloom, J. C. Jusem, and J. Ardizzone (1996), A multiyear global surface wind velocity dataset using SSM/I wind observations, *Bull. Am. Meteorol. Soc.*, *77*, 869–882.

Bhat, G. S. (2001), BOBMEX: The Bay of Bengal Monsoon Experiment, *Bull. Am. Meteorol. Soc.*, *82*, 2217–2243.

Bishop, J. K. B., W. B. Rossow, and E. G. Dutton (1997), Surface solar irradiance from the International Satellite Cloud Climatology Project 1983–1991, *J. Geophys. Res.*, *102*, 6883–6910.

Burton, J. D., (Ed.) (1988), River inputs to the ocean systems: Status and recommendations for research, final report of SCOR Working Group 46, 26 pp., U.N. Educ., Sci. and Cult. Org., Paris.

Cane, M. A. (1979), Response of an equatorial ocean to simple wind stress patterns. 1. Model formulation and analytic results, *J. Mar. Res.*, *37*, 233–252.

Chen, D., L. M. Rothstein, and A. J. Busalacchi (1994), A hybrid vertical mixing scheme and its application to tropical ocean models, *J. Phys. Oceanogr.*, *24*, 2156–2179.

Clarke, A. J., and X. Liu (1994), Interannual sea-level in the northern and eastern Indian-Ocean, *J. Phys. Oceanogr.*, *24*, 1224–1235.

Delcroix, T., and R. Murtugudde (2002), Sea surface salinity changes in the East China Sea during 1997–2001: Influence of the Yangtze River, *J. Geophys. Res.*, *107*(C12), 8008, doi:10.1029/2001JC000893.

Duchon, C. E. (1979), Lanczos filter in one and two dimensions, *J. Appl. Meteorol.*, *18*, 1016–1022.

Ferranti, L., J. M. Slingo, T. N. Palmer, and B. J. Hoskins (1997), Relations between interannual and intraseasonal monsoon variability as diagnosed from AMIP integrations, *Q. J. R. Meteorol. Soc.*, *123*, 1323–1357.

Gualdi, S., A. Navarra, and G. Tinarelli (1999), The interannual variability of the Madden-Julian Oscillation in an ensemble of GCM simulations, *Clim. Dyn.*, *15*, 643–658.

Hackert, E. C., A. J. Busalacchi, and R. Murtugudde (2001), A wind comparison study using an ocean general circulation model for the 1999–1998 El Nino, *J. Geophys. Res*, *106*, 2345–2362.

Han, W., and J. P. McCreary Jr. (2001), Modeling salinity distribution in the Indian Ocean, *J. Geophys. Res.*, *106*, 859–877.
Han, W. Q., and P. J. Webster (2002), Forcing mechanisms of sea level interannual variability in the Bay of Bengal, *J. Phys. Oceanogr.*, *32*, 216–239.
Han, W. Q., D. M. Lawrence, and P. J. Webster (2001), Dynamical response of equatorial Indian Ocean to intraseasonal winds: Zonal flow, *Geophys. Res. Lett.*, *28*, 4215–4218.
Hendon, H. H., C. D. Zhang, and J. D. Glick (1999), Interannual variation of the Madden-Julian Oscillation during austral summer, *J. Clim.*, *12*, 2538–2550.
Howden, S. D., and R. Murtugudde (2001), Effects of river inputs into the Bay of Bengal, *J. Geophys. Res.*, *106*, 19,825–19,843.
Jones, C., L. M. V. Carvalho, R. W. Higgins, D. E. Waliser, and J.-K. E. Schemm (2003), Climatology of tropical intraseasonal convective anomalies: 1979–2002, *J. Clim.*, *17*, 523–539.
Kang, I. S., C. H. Ho, Y. K. Lim, and K. M. Lau (1999), Principal modes of climatological seasonal and intraseasonal variations of the Asian summer monsoon, *Mon. Weather Rev.*, *127*, 322–340.
Kemball-Cook, S., and B. Wang (2001), Equatorial waves and air-sea interaction in the Boreal summer Intraseasonal Oscillation, *J. Clim.*, *14*, 2923–2942.
Kemball-Cook, S., B. Wang, and X. Fu (2002), Simulation of the ISO in the ECHAM4 model: The impact of coupling with an ocean model, *J. Atmos. Sci.*, *59*, 1433–1453.
Kessler, W. S., and R. Kleeman (2000), Rectification of the Madden-Julian Oscillation into the ENSO cycle, *J. Clim.*, *13*, 3560–3575.
Knox, R. A. (1976), Long series of measurements of Indian-Ocean equatorial currents near Addu Atoll, *Deep Sea Res.*, *23*, 211–221.
Knox, R. A. (1981), Time variability of Indian-Ocean Equatorial Currents, *Deep Sea Res. Part A*, *28*, 291–295.
Kraus, E. B., and J. S. Turner (1967), A one-dimensional model of seasonal thermocline. Part II. General theory and its consequences, *Tellus*, *19*, 98–105.
Lawrence, D. M., and P. J. Webster (2001), Interannual variations of the intraseasonal oscillation in the south Asian summer monsoon region, *J. Clim.*, *14*, 2910–2922.
Levitus, S. (1994), *Climatological Atlas of the World Ocean*, Natl. Oceanic and Atmos. Admin., Silver Spring, Md.
Loschnigg, J., and P. J. Webster (2000), A coupled ocean-atmosphere system of SST modulation for the Indian Ocean, *J. Clim.*, *13*, 3342–3360.
Luyten, J. R., M. Fieux, and J. Gonella (1980), Equatorial currents in the western Indian-Ocean, *Science*, *209*, 600–603.
Matsuno, T. (1966), Quasi-geostrophic motions in the equatorial area, *J. Meteorol. Soc. Jpn.*, *44*, 25–43.
McCreary, J. P., P. K. Kundu, and R. L. Molinari (1993), A numerical investigation of dynamics, thermodynamics and mixed-layer processes in the Indian-Ocean, *Prog. Oceanogr.*, *31*, 181–244.
Murtugudde, R., A. J. Busalacchi, and J. Beauchamp (1998), Seasonal-to-interannual effects of the Indonesian throughflow on the tropical Indo-Pacific Basin, *J. Geophys. Res.*, *103*, 21,425–21,441.
Myers, D., and D. E. Waliser (2003), Three dimensional water vapor and cloud variations associated with the Madden-Julian Oscillation during Northern Hemisphere winter, *J. Clim.*, *16*, 929–950.
Potemra, J. T., M. E. Luther, and J. J. Obrien (1991), The seasonal circulation of the upper ocean in the Bay of Bengal, *J. Geophys. Res.*, *96*, 12,667–12,683.
Reppin, J., F. A. Schott, J. Fischer, and D. Quadfasel (1999), Equatorial currents and transports in the upper central Indian Ocean: Annual cycle and interannual variability, *J. Geophys. Res.*, *104*, 15,495–15,514.
Reynolds, R. W., and T. M. Smith (1994), Improved global sea-surface temperature analyses using optimum interpolation, *J. Clim.*, *7*, 929–948.
Rossow, W. B., and R. A. Schiffer (1991), ISCCP cloud data products, *Bull. Am. Meteorol. Soc.*, *72*, 2–20.
Schott, F., J. Reppin, J. Fischer, and D. Quadfasel (1994), Currents and transports of the Monsoon Current south of Sri Lanka, *J. Geophys. Res.*, *99*, 25,127–25,141.
Sengupta, D., and M. Ravichandran (2001), Oscillations of Bay of Bengal sea surface temperature during the 1998 summer monsoon, *Geophys. Res. Lett.*, *28*, 2033–2036.
Sengupta, D., B. N. Goswami, and R. Senan (2001a), Coherent intraseasonal oscillations of ocean and atmosphere during the Asian summer monsoon, *Geophys. Res. Lett.*, *28*, 4127–4130.
Sengupta, D., R. Senan, and B. N. Goswami (2001b), Origin of intraseasonal variability of circulation in the tropical central Indian Ocean, *Geophys. Res. Lett.*, *28*, 1267–1270.
Shinoda, T., and H. H. Hendon (2001), Upper-ocean heat budget in response to the Madden-Julian Oscillation in the western equatorial Pacific, *J. Clim.*, *14*, 4147–4165.
Slingo, J. M., D. P. Rowell, K. R. Sperber, and E. Nortley (1999), On the predictability of the interannual behaviour of the Madden-Julian Oscillation and its relationship with El Nino, *Q. J. R. Meteorol. Soc.*, *125*, 583–609.
Sperber, K. R., J. M. Slingo, and H. Annamalai (2000), Predictability and the relationship between subseasonal and interannual variability during the Asian summer monsoon, *Q. J. R. Meteorol. Soc.*, *126*, 2545–2574.
Sprintall, J., A. L. Gordon, R. Murtugudde, and R. D. Susanto (2000), A semiannual Indian Ocean forced Kelvin wave observed in the Indonesian seas in May 1997, *J. Geophys. Res.*, *105*, 17,217–17,230.
Vecchi, G. A., and D. E. Harrison (2002), Monsoon breaks and subseasonal sea surface temperature variability in the Bay of Bengal, *J. Clim.*, *15*, 1485–1493.
Waliser, D., Z. Zhang, K. M. Lau, and J. H. Kim (2001), Interannual sea surface temperature variability and the predictability of tropical intraseasonal variability, *J. Atmos. Sci.*, *58*, 2595–2614.
Waliser, D. E., R. Murtugudde, and L. E. Lucas (2003), Indo-Pacific Ocean response to atmospheric intraseasonal variability: 1. Austral summer and the Madden-Julian Oscillation, *J. Geophys. Res.*, *108*(C5), 3160, doi:10.1029/2002JC001620.
Wang, B., and H. Rui (1990), Synoptic climatology of transient tropical intraseasonal convection anomalies—1975–1985, *Meteorol. Atmos. Phys.*, *44*, 43–61.
Wang, B., and X. H. Xu (1997), Northern Hemisphere summer monsoon singularities and climatological Intraseasonal Oscillation, *J. Clim.*, *10*, 1071–1085.
Webster, P. J., et al. (2002), The jasmine pilot study, *Bull. Am. Meteorol. Soc.*, *83*, 1603–1630.
Wu, M. L. C., S. Schubert, I. S. Kang, and D. E. Waliser (2002), Forced and free intra-seasonal variability over the south Asian monsoon region simulated by 10 AGCMs, *J. Clim.*, *15*, 2862–2880.
Wyrtki, K. (1973), Equatorial jet in Indian Ocean, *Science*, *181*, 264–266.
Xie, P. P., and P. A. Arkin (1997), Global precipitation: A 17-year monthly analysis based on gauge observations, satellite estimates, and numerical model outputs, *Bull. Am. Meteorol. Soc.*, *78*, 2539–2558.

L. E. Lucas and D. E. Waliser, Marine Sciences Research Center, State University of New York at Stony Brook, Endeavor Hall 205, Stony Brook, NY 11794-5000, USA. (duane.waliser@sunysb.edu)
R. Murtugudde, Earth System Science Interdisciplinary Center, University of Maryland, College Park, MD 20742, USA.